Dynamics of Ligand Binding to Myoglobin†

R. H. Austin, K. W. Beeson, L. Eisenstein, H. Frauenfelder,*
and I. C. Gunsalus

ABSTRACT: Myoglobin rebinding of carbon monoxide and dioxygen after photodissociation has been observed in the temperature range between 40 and 350 K. A system was constructed that records the change in optical absorption at 436 nm smoothly and without break between 2 μsec and 1 ksec. Four different rebinding processes have been found. Between 40 and 160 K, a single process is observed. It is not exponential in time, but approximately given by $N(t) = (1 + t/t_0)^{-n}$, where t_0 and n are temperature-dependent, ligand-concentration independent, parameters. At about 170 K, a second and at 200 K, a third concentration-independent process emerge. At 210 K, a concentration-dependent process sets in. If myoglobin is embedded in a solid, only the first three can be seen, and they are all nonexponential. In a liquid glycerol–water solvent, rebinding is exponential. To interpret the data, a model is proposed in which the ligand molecule, on its way from the solvent to the binding site at the ferrous heme iron, encounters four barriers in succession. The barriers are tentatively identified with known features of myoglobin. By computer-solving the differential equation for the motion of a ligand molecule over four barriers, the rates for all important steps are obtained. The temperature dependences of the rates yield enthalpy, entropy, and free-energy changes at all barriers. The free-energy barriers at 310 K indicate how myoglobin achieves specificity and order. For carbon monoxide, the heights of these barriers increase toward the inside; carbon monoxide consequently is partially rejected at each of the four barriers. Dioxygen, in contrast, sees barriers of about equal height and moves smoothly toward the binding site. The entropy increases over the first two barriers, indicating a rupturing of bonds or displacement of residues, and then smoothly decreases, reaching a minimum at the binding site. The magnitude of the decrease over the innermost barrier implies participation of heme and/or protein. The nonexponential rebinding observed at low temperatures and in solid samples implies that the innermost barrier has a spectrum of activation energies. The shape of the spectrum has been determined; its existence can be explained by assuming the presence of many conformational states for myoglobin. In a liquid at temperatures above about 230 K, relaxation among conformational states occurs and rebinding becomes exponential.

1. Myoglobin and Its Ligands

Myoglobin (Mb),[1] a globular protein of about 17200 molecular weight and 153 amino acids containing one protoheme, plays an important role in the mammalian cell where it stores (Theorell, 1934) and transports (Wittenberg, 1970) oxygen and possibly also carries energy (Hills, 1973). An understanding of the reactions of ferrous Mb with ligands, particularly dioxygen and carbon monoxide, is desirable because, as the simplest protein capable of reversible oxygenation, it can serve as a prototype for more complex systems. Dynamic studies are particularly meaningful because the primary and tertiary structures have been determined (Kendrew et al., 1958) and many properties of the active center are known (Weissbluth, 1974).

The reactions of various ligands with Mb have been investigated extensively with stopped-flow, flash-photolysis, and T-jump techniques. The pioneering work has been performed by Gibson (Gibson, 1956); his and later experiments are reviewed and referenced in the monograph by Antonini and Brunori (Antonini and Brunori, 1971). Our study of the binding of O_2 and CO to sperm whale Mb by flash photolysis extends earlier work in three directions, temperature, time, and dynamic range. Phenomena change so rapidly with temperature that measurements are needed at 10-K intervals between 40 and 350 K. Since processes can encompass more than nine orders of magnitude in time, we constructed a system capable of recording over this range in one sweep. Our equipment records data over more than three orders of magnitude in optical density and we thus can see even processes with relative intensities of less than 1%.

The experimental data are rich and complex but they can be unraveled to give a coherent description of the dynamics of ligand binding to Mb. The essential *experimental* fact is the discovery of four distinct processes (Austin et al., 1973). The central *interpretative* assumption is that ligand binding is governed by successive barriers (Frauenfelder, 1973). The four processes depend differently on temperature and concentration; thus all essential parameters of our model can be determined and all observed features can be understood.

† From the Department of Physics and the Department of Biochemistry, University of Illinois at Urbana—Champaign, Urbana, Illinois 61801. *Received August 7, 1974.* This work was supported in part by the U.S. Department of Health, Education, and Welfare under Grants No. GM 18051 and No. AM 00562, and the National Science Foundation under Grant No. GB 41629X.

* To whom correspondence should be addressed at the Department of Physics.

[1] Abbreviations, symbols, and units: Mb, ferrous sperm whale myoglobin; L, ligand molecule; PVA, poly(vinyl alcohol). Processes I–IV are defined in section 4, barriers I–IV and wells A–E in Figure 11. $N(t)$ denotes the fraction of Mb molecules that have not rebound a ligand at the time t after photodissociation. $N_a(t)$, for instance, gives the probability of finding a ligand molecule in well A at time t, k_{ab} is the first-order rate for transitions from well A to B. Second-order rates are denoted by primes, for instance k_{ed}' (eq 6). E_{ab} and A_{ab}, for instance, denote the activation energy and the frequency factor for the transition from well A to B. Energies are given in kcal/mol; 1 kcal/mol = 0.043 eV = 4.18 kJ/mol. Entropies are given in terms of the dimensionless ratio S/R, where R = 1.99 cal mol^{-1} K^{-1} is the gas constant.

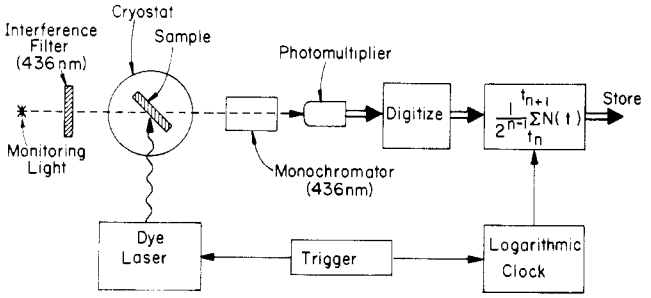

FIGURE 1: Flash photolysis system designed to observe processes that extend over many decades in time.

Preliminary data indicate that the processes discussed here for Mb occur also in other heme proteins, namely hemoglobin, the separated hemoglobin monomers, cytochrome P450, and carboxymethylated cytochrome *c*. Thus our model may well apply to many biomolecules. We will show that the rate constants for ligand binding at physiological temperatures are determined by multiple barriers whose characteristics can be separated only if photodissociation is studied in the entire temperature range from about 40 to 320 K. Low-temperature experiments are thus necessary to understand the physiological behavior of heme proteins.

Section 2 describes the experimental approach, section 3 the results. In section 4, we introduce a model capable of explaining all observed features. The data evaluation follows in sections 5–8; activation energies and entropies are collected in section 9. Section 10 provides a summary.

2. Experimental Approach

The idea underlying studies of heme protein dynamics by flash photolysis is simple. Consider Mb with bound ligand L, denoted by MbL. Irradiation with light absorbed by MbL breaks the bond; L dissociates from Mb and later rebinds. Photodissociation and rebinding can be followed optically. The Soret absorption band is at 434 nm for Mb, 423 nm for MbCO, and 418 nm for MbO_2; the absorbancy near 434 nm thus indicates the fraction of Mb molecules free of L. The sample is placed in a cryostat with optical windows and the transmission at 436 nm monitored with a photomultiplier. Photodissociation is initiated with a 590-nm flash of 2 μsec duration from a 0.5-J rhodamine 6G–methanol dye laser. Sample heating by the laser flash is less than 0.5 K at 300 K. A long-pass filter, 540–3000 nm, between laser and sample prevents the laser from disturbing the monitoring at 436 nm.

Customarily the photomultiplier output is fed into a storage oscilloscope and the data are taken from the scope tracing. Since the time bases of oscilloscopes are linear, only a limited range in time is observed after a single flash and data from several flashes must be pieced together for complete coverage. Such an approach is time consuming and introduces errors. We therefore have developed a system for smooth observation of ligand rebinding over nine decades in time (R. H. Austin et al., to be published). The approach and components are explained with Figure 1. A trigger simultaneously fires the laser and starts a "logarithmic clock". The flash illuminates the sample in the cryostat and photodissociates MbL. Rebinding is followed by detecting the transmitted 436-nm beam with a photomultiplier. The light source, a tungsten–iodide lamp, is stabilized by monitoring the intensity with a temperature-controlled photodiode. After triggering, the crystal-controlled logarithmic clock emits signals in exponentially increasing intervals. The first m intervals have a length Δ, the second m intervals 2Δ, the third $2^2\Delta$, and the nth set of m intervals $2^{n-1}\Delta$. Here m is an integer adjustable from 1 to 10. The photomultiplier output is integrated over time Δ, digitized, and summed over a given interval of length $2^{n-1}\Delta$. The sum is divided by 2^{n-1} and the result stored. Thus, even though the interval length increases exponentially with time, a constant input signal results in a constant output. In the present system, the maximum $n = 24$ and the minimum $\Delta = 2$ μsec. If the first interval is 2 μsec, the longest interval is $2^{24-1} \times 2$ μsec = 16.8 sec, and the entire measurement extends over $m(2^n - 1)\Delta$ or 336 sec when $m = 10$. Kinetics at longer times can be observed by increasing the length Δ of the basic interval. From the observed intensity as a function of time, the optical density is computed. The result is expressed in terms of $N(t)$, the fraction of Mb molecules that have not rebound a ligand molecule at time t after the flash.

Our system is capable of observing $N(t)$ over an intensity range of more than three orders of magnitude. To avoid the inability of most photomultipliers to reproduce rapid and large changes in intensity well, an anti-hysteresis photomultiplier, RCA Type 4837, is used. The transient response to a fast increase in absorbance was tested by switching off a green LED (light emitting diode) with a mercury relay in the presence of a steady light. The overshoot or undershoot after the LED shut-off was less than 0.01%.

Samples were prepared from Sigma Type 2 sperm whale Mb, dissolved in 0.1 *M* phosphate (pH 7.6), and filtered through 0.2-μm filters. (Further purification by ion-exchange chromatography did not affect results.) Three types of ferrous Mb samples were used: buffered aqueous solution, glycerol–water solution, and Mb embedded in poly(vinyl alcohol) (PVA). Reduction was accomplished by adding freshly prepared anaerobic solutions of sodium dithionite to anaerobic samples. Samples were rendered anaerobic by stirring in an argon atmosphere. The dithionite concentration was five times the Mb concentration for CO samples. For O_2, a twofold excess of dithionite was added for initial reduction of Mb, then removed by stirring in the desired O_2 atmosphere. To check for dithionite effects in the oxygen runs an enzymatic reduction system (NADPH, spinach ferredoxin–NADP oxidoreductase, and ferredoxin) was also employed, with identical results.

CO or O_2 was introduced by stirring the samples in a thermostated cell exposed to the desired gaseous atmosphere. For CO equilibration, at 20°C, 10 min of stirring was sufficient for aqueous solutions; the viscous glycerol samples required 1 hr for saturation. The O_2 samples were prepared at 5°C. The oxygenated Mb was stabilized by adding 10 m*M* EDTA. The aqueous O_2 solutions were equilibrated for 0.5 hr while for glycerol runs a concentrated aqueous Mb sample was oxygenated and then added to the previously equilibrated glycerol, thus keeping equilibration time to a minimum.

The aqueous samples contained 100 m*M* phosphate buffer (pH 7.6) with a freezing point of 270 K. The glycerol samples contained 3 ml of reagent grade glycerol and 1 ml of 100 m*M* phosphate buffer (pH 7.6). The PVA samples contained 10% by weight of poly(vinyl alcohol), dissolved in 1 m*M* phosphate buffer by boiling, and cooled to room temperature. The Mb was then added, reduced, and equilibrated with the desired gas, and the sample was placed in a desiccator under the desired gaseous atmosphere and allowed to dry to a hard film. The process took several days.

Several concentrations of myoglobin were used in the experiments. For temperatures above 200 K, 10 μM Mb was placed in a 1-cm long cell. For measurements extending below 200 K, a 0.5-mm thick cell containing 200 μM Mb minimized problems with cracking of the sample. With such a short cell, light transmission after cracking was reduced by only about a factor 5. Thus a monitoring light level could be chosen that had no measurable effect on the kinetics.

3. Results

Flash photolysis experiments by Chance et al. (Chance et al., 1965) had already shown in 1965 that rebinding of CO to heme proteins after a photoflash can occur at a temperature of 77 K. Our preliminary work (Austin et al., 1973, 1974) revealed three different processes in the temperature range between 40 and 300 K. The present measurements imply four different processes, denoted by I–IV and distinguished by their temperature and concentration dependences.[2] Below about 180 K, only process I appears. At intermediate temperatures, between about 180 and 280 K, up to four different processes can be seen. Above about 280 K, only one process (III or IV, depending on conditions) remains directly observable. Processes I–III are independent of the ligand concentration and IV is proportional to it.

In each experiment, we measure the intensity of the transmitted beam as a function of time and then compute $N(t)$, the fraction of Mb molecules that have not rebound a ligand molecule at the time t after a flash. Usually, log $N(t)$ is plotted vs. t. However, our rebinding data extend over many orders of magnitude in time, and a plot of log $N(t)$ vs. t either compresses the fast or eliminates the slow part. Consequently, nearly all data are presented by plotting log $N(t)$ vs. log t. In a log–log plot a straight line corresponds to a power law; $N(t) \propto t^{-n}$ leads to log $N(t) \propto -n$ log t. An exponential, $N(t) = \exp(-kt)$, leads to log $N(t)$ $= -0.434 \exp[2.30(\log k + \log t)]$ so that the shape of log $N(t)$ vs. log t does not depend on the rate k; k only determines the position along the log t axis.[3] After these preliminary remarks, we present the experimental results. The curves in Figures 2–9 form a small selection from all the data that were taken; additional information, such as the concentration dependence of the various processes, is given in the text.

Low-Temperature Region. Rebinding data for MbCO and MbO_2 below 200 K are given in Figures 2a, 2b, and 4a. In taking these data, two precautions are observed. (1) Between any two runs, the sample is warmed up to at least 120 K in order to allow all ligand molecules to rebind before the next photodissociation.[4] (2) The intensity of the monitoring light is adjusted so that ligand molecules that have rebound are not driven off again.

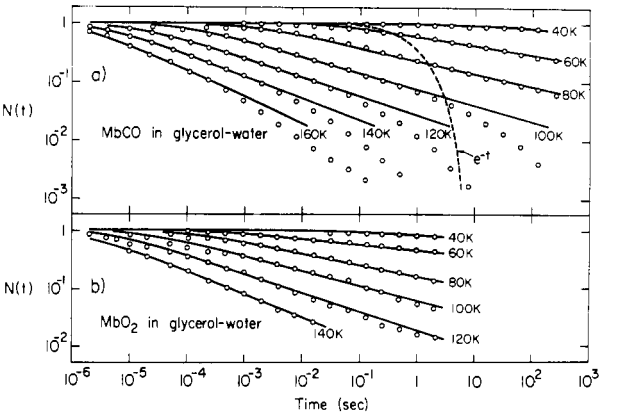

FIGURE 2: (a) Rebinding of CO to Mb after photodissociation below 160 K. The solvent is glycerol–water (3:1, v/v). We denote this low-temperature process by I; the solid lines are least-squares fit to the data with $N(t) = (1 + t/t_0)^{-n}$. At each temperature, the two parameters t_0 and n are determined. The dashed line is an exponential with mean return time 1 sec. Exponentials with other mean times are obtained by shifting the dashed curve along the t axis. (b) Rebinding of O_2 to Mb after photodissociation.

Figures 2a, 2b, and 4a show only one rebinding process below about 180 K; we denote it by I. It is independent of the ligand molecule concentration in the solvent and depends only weakly on solvent nature. The shape of $N(t)$ is remarkable. A sample exponential is shown in Figure 2; the experimental curves deviate markedly from exponentials and are much closer to power laws. Indeed, for $N(t) > 0.05$, all experimental curves below about 180 K can be approximated by expressions of the form

$$N_0^{I}(t) = (1 + t/t_0)^{-n} \qquad (1)$$

where parameters t_0 and n change smoothly with temperature. The parameter n gives the slope of $N(t)$ in the "straight" part of the log–log plot shown in Figure 2a; t_0 very approximately gives the time where $N(t)$ breaks away from the horizontal. Computer fits of eq 1 to the observed points are shown in Figure 2 as solid lines; these fits yield values of t_0 and n for each temperature. Comparison of Figure 2a and b indicates that O_2 and CO rebind similarly; both ligands display the same nonexponential behavior, but O_2 is somewhat faster. At a first glance, the curves in Figures 2a and 4a appear identical. A closer look, however, shows that the solvent affects the shape of $N(t)$ somewhat: the curves in PVA break away more gradually from the horizontal and drop off less rapidly at long times.

In Figure 3, the result of a multiple flash experiment is shown. The sample is kept at 70 K and flashing is repeated every 18 sec, before all CO molecules have rebound.

Intermediate and High Temperature Regions. Figure 4 shows the rebinding of CO to Mb after photodissociation for MbCO embedded in PVA. The sample is solid up to at least 370 K. Below 180 K, only process I is present. Above 180 K, process II emerges and it constitutes the major fraction of $N(t)$ at 230 K. At 240 K, process III appears. As the temperature is further increased, III becomes dominant. All three processes are nonexponential and independent of CO concentration.

Figure 5 concerns MbCO in water. At low temperatures, only partially shown, processes I–III appear as in PVA, nonexponential and CO-concentration independent. Above the melting point, $N(t)$ becomes slower, exponential, and with a return rate that is proportional to the CO concentra-

[2] The classification introduced here differs from our earlier one (Austin et al., 1973) and is based on more data.

[3] We use the independence of the shape on k to construct a simple tool for rapid preliminary data evaluation. By cutting a cardboard exponential $-0.434 \exp(2.30 \log t)$ and shifting it along the log t axis, we check if a part of the experimental curve can be approximated by an exponential; if yes, the position of the sample exponential gives a preliminary value of k.

[4] If this precaution is neglected, the long-time components do not rebind. The next flash then can drive off only the ligand molecules that have returned quickly; an apparent temperature dependence of the quantum yield and a short recombination time are observed. This effect may explain the discrepancy between our data and those of Iizuka et al. (Iizuka et al., 1974).

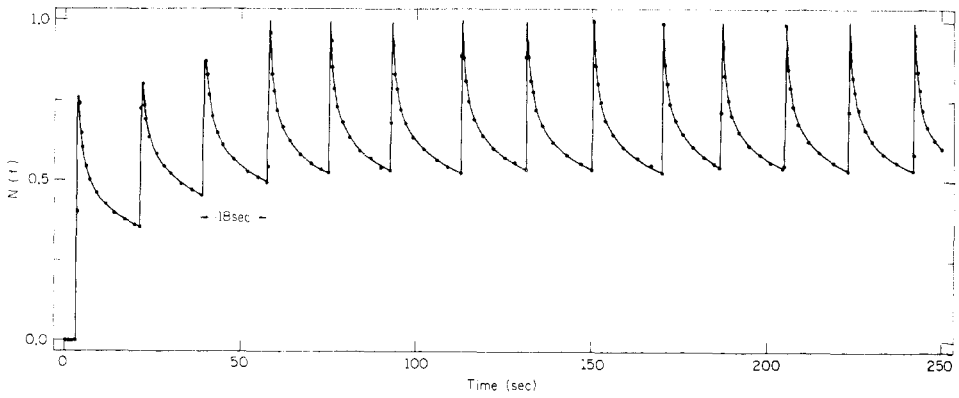

FIGURE 3: Multiple flash experiment: $N(t)$ is plotted vs. time. Sample: MbCO in glycerol-water (3:1, v/v). T = 70 K. Flashing is repeated approximately every 18 sec.

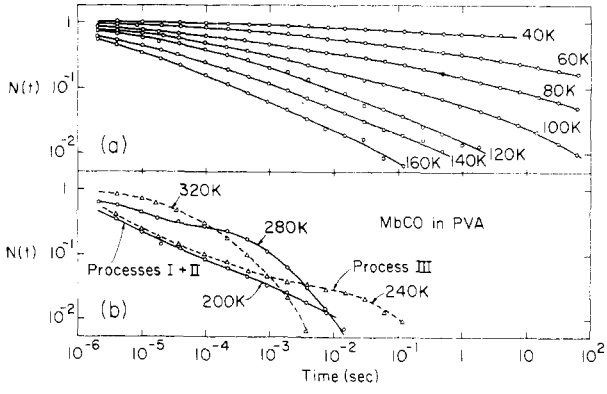

FIGURE 4: Rebinding of CO to Mb after photodissociation. MbCO is embedded in poly(vinyl alcohol); the solvent is solid up to at least 350 K. (a) Low-temperature region, where only process I is visible. (b) At temperatures above 200 K, three processes can be seen; all are nonexponential. Lines are drawn to guide the eye.

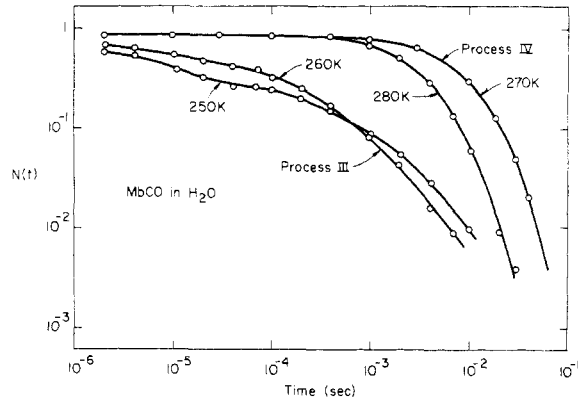

FIGURE 5: Rebinding of CO to Mb in water (ice). Above the melting point, 270 K, the ligand concentration-proportional and exponential process IV is seen. Below the freezing point, diffusion into the solvent is inhibited and the faster, concentration-independent and nonexponential, process III appears. At lower temperatures, I and II, not shown here, are similar to the corresponding processes in Figures 2 and 4. [CO] = 10^{-4} M.

tion in the solvent after the flash. We identify this process with IV.

Figure 5 suggests that process IV, which implies ligand diffusion into the solvent, takes place if the surrounding of Mb is liquid. More information on this point is obtained by observing a PVA sample during solidification (Figure 6). Immediately after preparation, while the sample is still liquid, the concentration-dependent exponential process IV is present. After about 2 hr, IV vanishes and is replaced by the faster and concentration-independent process III. The sample at this point is still liquid and III is exponential. If the sample is prevented from further drying, III remains exponential. If the PVA sample is hardened by drying, III becomes nonexponential as indicated in Figure 6 and also in Figure 4b.

To study process IV in more detail, we use solvents with low melting (glass) points, for instance glycerol-water (3:1 by volume) as in Figure 7. Here, only I exists up to about 180 K. Between 180 and 200 K, I and II are present simultaneously. At about 200 K, III sets in, and at about 210 K, IV appears. I-III are independent, IV is proportional to CO concentration. The decomposition of $N(t)$ at 215 K into four components, done by computer, is shown in Figure 8. The curves I-IV do not depend on the glass transition temperature of the glycerol-water solvent (Bohon and Conway, 1972).

So far, we have concentrated on CO. Figure 9 gives rebinding data for O_2 to Mb in glycerol-water. Only processes I, II, and IV can be seen clearly; I and II are independent of, IV is proportional to, the O_2 concentration.

4. A Model

The experimental curves in the previous section demonstrate that ligand binding to Mb is complex. To understand and evaluate the data, a model is needed. We have constructed one that reproduces all experimental data and can be correlated with structural features of Mb. The salient features are multiple energy barriers, interplay of entropy and enthalpy, presence of an energy spectrum, and occurrence of conformational relaxation. It is possible that equivalent models exist, but we believe that they will contain the same central features.

The data in section 3 show four processes in the rebinding of ligands to Mb after photodissociation.[5] Processes I-III are independent of ligand concentration. IV is proportional to the ligand concentration and slower than a diffusion-limited process. The rates of all four processes are thus most likely governed by barriers. Four barriers are needed to produce four distinct processes. They can be in series, parallel,

[5] The number four is not universal. In some other proteins, we find fewer processes; in MbCO, there is evidence for a fifth one. It is likely that further improvements in equipment will lead to the discovery of additional processes.

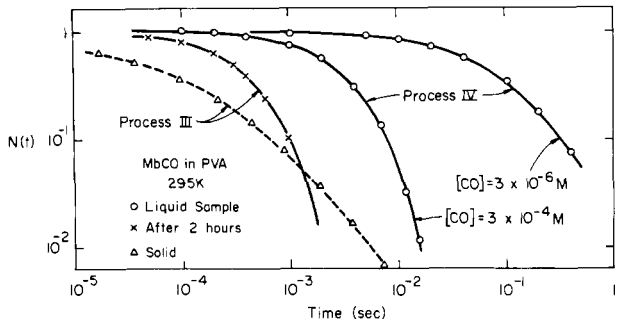

FIGURE 6: Rebinding of CO to Mb in PVA. The curves denoted by IV are obtained in a freshly prepared sample that is still liquid. After about 2-hr drying time, IV disappears and the exponential, but CO independent and faster, process III appears. On complete drying, when PVA becomes solid, the nonexponential curve III is observed.

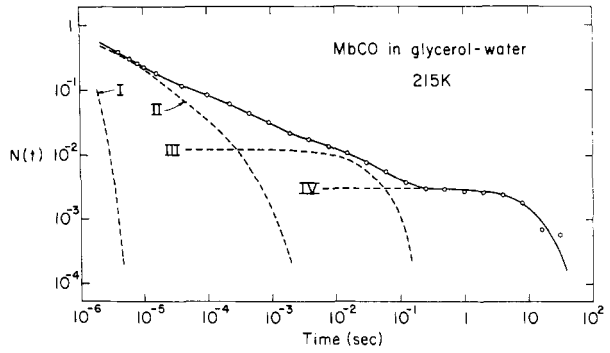

FIGURE 8: Separation of $N(t)$ for T = 215 K into the components I–IV. MbCO in glycerol-water, 3:1, v/v. [CO] = 3 × 10^{-5} M. The figure also shows some tentative evidence for a fifth process between II and III.

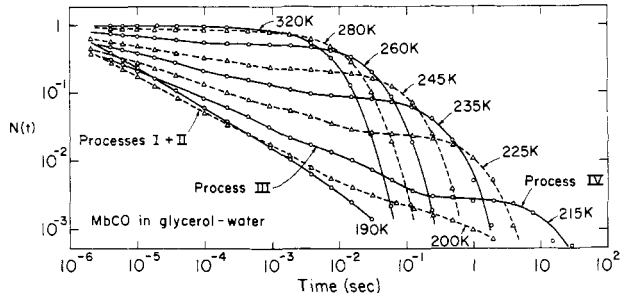

FIGURE 7: Rebinding of CO to Mb after photodissociation. Solvent: glycerol-water, 3:1, v/v. [CO] = 3 × 10^{-5} M. All four processes discussed in the text are recognizable.

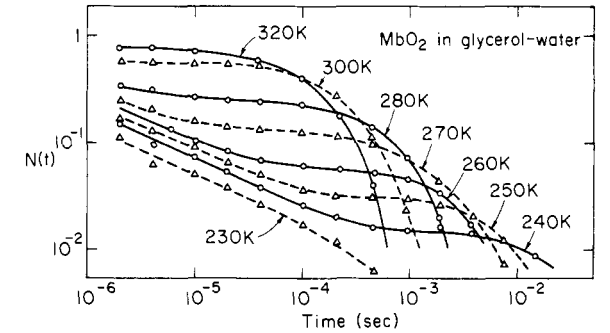

FIGURE 9: Rebinding of O_2 to Mb. Solvent: glycerol-water, 3:1, v/v. [O_2] = 6 × 10^{-5} M. Processes I, II, and IV are indicated; III is not very prominent and is neglected.

or mixed; they can be caused by different parts of the system biomolecule–solvent, or by conformational transformations. We postulate four barriers in sequence.

Four barriers in sequence can be discussed without referring to the actual physical system, but we find it constructive to think in terms of a concrete model, as sketched in Figure 10. The structure of Mb shows the prosthetic group, protoheme, in a pocket of the protein with the iron approximately 1 nm from the protein surface (Watson, 1968). The pocket is lined with nonpolar groups; the polar residue of the proximal histidine His-64 is close to the heme iron. The protein is surrounded by the hydration shell, a layer of water molecules about 0.4 nm thick with properties different from bulk water (Cooke and Kuntz, 1974, Kuntz and Kauzmann, 1974). The Mb-solvent system thus can be pictured as in Figure 10. This figure makes it plausible that a ligand molecule on its way to the binding site from the solvent can encounter multiple barriers. We will discuss the properties of the four barriers and a possible identification in section 10; here we assume that the potential (enthalpy) seen by a ligand molecule on its approach to the iron looks as in Figure 11. The abscissa represents the reaction coordinate. In each well, the ligand thermalizes before making the next move.

The processes that a ligand molecule can undergo can be described with Figures 10 and 11. Entering from the solvent corresponds to *association.* In *dissociation* a ligand molecule initially bound to the iron atom in well A moves to the outside by thermally overcoming all barriers. In *photodissociation,* L initially also occupies well A. An incident photon excites the iron atom into an antibonding state, changing the attractive well A into a repulsive one (Zerner et al., 1966), and L moves into well B. Processes I–IV in section 3 can also be interpreted with the help of Figures 10 and 11. Immediately after photodissociation, L is in well B and the following processes can take place: I, L rebinds directly from B to A; II, L jumps over barrier II to well C; from there it rebinds by first returning to B and then to A; III, L jumps to D via C and then rebinds, D → C → B → A. IV, L jumps to E via C and D and diffuses into the solvent. All ligand molecules in the solvent then compete for the vacant binding site via the chain E → D → C → B → A. In this interpretation, processes I–III are independent of ligand concentration, IV is proportional to it. One feature observed in section 3 is thus reproduced. A second striking feature, the appearance of only one process below about 180 K, is intuitively plausible. At very low temperatures, the Mb molecule is "frozen shut" and only intramolecular processes occur. At high temperatures, the ligand can leave the Mb molecule. To understand this feature in more detail, consider the two-barrier situation obtained in Figure 11 if barrier III is very high. A ligand in well B then can either rebind directly (process I), or first move to C and then rebind via B (process II). We assume that all rates obey Arrhenius equations

$$k(T) = Ae^{-E/RT} \tag{2}$$

A is a frequency factor, E an activation energy, and R = 1.99 cal mol^{-1} K^{-1} the gas constant. A and E are taken to be temperature independent. The ratio of transition rates from B to A and C is now determined by

$$\frac{k_{ba}}{k_{bc}} = \frac{A_{ba}}{A_{bc}} e^{(E_{bc}-E_{ba})/RT} \tag{3}$$

Here, k_{ba}, for instance, denotes the transition rate from B

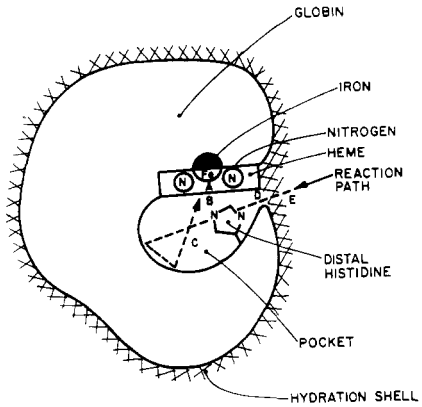

FIGURE 10: Binding of a ligand molecule to myoglobin. A possible reaction path is indicated by the dashed line. A tentative identification of the barriers and wells with known structural features of Mb is given in subsection 10.2.

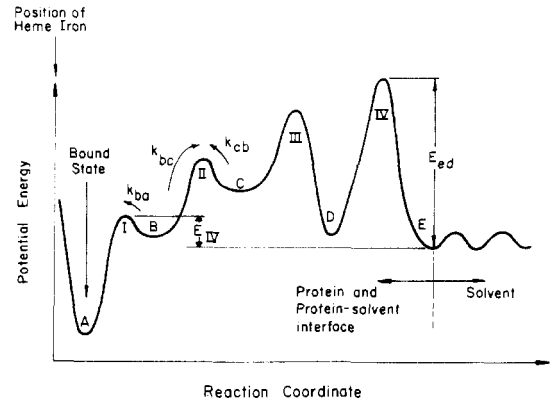

FIGURE 11: Potential encountered by a ligand molecule approaching the heme iron from the solvent. The barriers are numbered I–IV, the wells labeled A–E. The energy E_{ed}, for instance, measures the activation energy for the step E → D. The energy E_{IV} is defined by eq 48.

to A, E_{ba} is the activation energy, and A_{ba} the frequency factor for the same transition. The data evaluation in sections 5–8 indicates that

$$A_{ba}/A_{bc} \ll 1, \quad E_{bc} > E_{ba} \tag{4}$$

Consequently, k_{ba}/k_{bc} becomes large at low and tends to zero at high temperatures. At low temperatures, ligand molecules in pocket B rebind directly; at higher temperatures, they make the round trip via well C before rebinding. This argument thus can explain why only one process is present below about 180 K. To describe the occurrence of all four processes, the treatment must be extended to four barriers. A detailed comparison between model and experiment then requires the solution of the four coupled differential equations that describe the motion of a particle over the four barriers shown in Figure 11:

$$\begin{aligned} dN_a/dt &= -k_{ab}N_a + k_{ba}N_b \\ dN_b/dt &= k_{ab}N_a - k_{ba}N_b - k_{bc}N_b + k_{cb}N_c \\ dN_c/dt &= k_{bc}N_b - k_{cb}N_c - k_{cd}N_c + k_{dc}N_d \\ dN_d/dt &= k_{cd}N_c - k_{dc}N_d - k_{de}N_d + k_{ed}N_e \\ dN_e/dt &= k_{de}N_d - k_{ed}N_e \end{aligned} \tag{5}$$

Here, N_a denotes the probability of finding a ligand molecule in well A at time t and k_{ab} is the rate for transitions from well A to well B. $N(t)$, the quantity defined in section 3 as the fraction of Mb molecules that have not rebound a ligand, is given by $N(t) = 1 - N_a$. The equations are valid if the ligand concentration [L] in the solvent is sufficiently large so that process IV can be treated as a pseudo-first-order reaction and k_{ed} is a pseudo-first-order rate. Otherwise, k_{ed} must be replaced:

$$k_{ed} \rightarrow k_{ed}'[L] \tag{6}$$

where k_{ed}' is a second-order rate. We will restrict our discussion to the limiting case of high ligand concentrations.

Photodissociation moves the ligand molecules from well A to B so that

$$N_b(0) = 1, \quad N_a(0) = N_c(0) = N_d(0) = N_e(0) = 0 \tag{7}$$

In general, the solution of eq 5 must be done numerically. Dissociation is slow at all temperatures and satisfies $k_{ab} \ll k_{ba}$ so that we always set $k_{ab} = 0$ in eq 5. In the following sections we use eq 5 to deduce the various rates from the experimental data. The temperature dependence of the rates yields the activation energies and frequency factors of the four barriers. The approach rests on the crucial assumption that the Mb molecule does not undergo a major conformational transformation in the temperature range between 40 and 300 K, except for relaxation effects to be described in section 7. The fact that we can fit all data with a consistent set of energies and entropies supports the assumption, but further experiments will be needed to prove it unambiguously.

5. Direct Rebinding and Activation Energy Spectrum

At temperatures below about 180 K, only one process, identified with the direct return B → A (Figure 11), is observed. Direct rebinding implies $k_{bc} \ll k_{ba}$ and eq 5 reduces to a one-barrier problem:

$$dN_a/dt = k_{ba}N_b = k_{ba}(1 - N_a) \tag{8}$$

where we have assumed $k_{ab} = 0$. The solution of eq 8 with the initial condition eq 7 is an exponential:

$$N(k_{ba},t) = 1 - N_a = e^{-k_{ba}t} \tag{9}$$

The curves in Figures 2 and 4, however, are not exponentials, but closer to power laws, as expressed by eq 1. The observed shape and temperature dependence of these curves are explained (Austin et al., 1974) if the energy of barrier I is not sharp, but given by a distribution $g(E_{ba})$, where $g(E_{ba})$ denotes the probability of finding a Mb molecule with activation energy between E_{ba} and $E_{ba} + dE_{ba}$. For a distributed activation energy, eq 9 is generalized to read[6]

$$N(t) = \int_0^\infty dE_{ba}g(E_{ba})N(k_{ba},t) = \int_0^\infty dE_{ba}g(E_{ba})e^{-k_{ba}t} \tag{10}$$

where k_{ba} is related to the activation energy E_{ba} and the

[6] Nonexponential curves have been observed in many fields and their explanation in terms of integrals as in eq 10 dates back to at least 1913 (Wagner, 1913). Detailed theoretical treatments can be found in papers by Macdonald (1962, 1963, 1964) and Primak (1955).

frequency factor A_{ba} by eq 2.[7] We assume here that A_{ba} is independent of E_{ba}. Equation 2 gives $dE_{ba} = -RTdk_{ba}/k_{ba}$ and $N(t)$ becomes

$$N(t) = RT \int_0^{A_{ba}} dk_{ba}[g(k_{ba})/k_{ba}]e^{-k_{ba}t} \qquad (11)$$

By eq 2, the energy E_{ba} is related to k_{ba} by $E_{ba} = RT \ln (A_{ba}/k_{ba})$. For a given frequency factor A_{ba}, the distribution function $g(E_{ba})$ thus can be considered a function of k_{ba}. We will write it alternately as $g(E_{ba})$ or $g(k_{ba})$, depending on whether we express it in terms of E_{ba} or k_{ba}. In either case, g is different from the function $f(k_{ba})$ described in footnote 7.

For the times involved in our measurements, A_{ba} satisfies the relation $A_{ba}t \gg 1$. The upper limit of the integral can then be taken to be infinite and $N(t)$ becomes the Laplace transform of $g(k_{ba})/k_{ba}$:

$$N(t) = RT \int_0^{\infty} dk_{ba} \frac{g(k_{ba})}{k_{ba}} e^{-k_{ba}t} = RT\mathcal{L}\{g(k_{ba})/k_{ba}\} \qquad (12)$$

From the measured $N(t)$, the distribution function can be determined in terms of k_{ba} by the inverse Laplace transform

$$g(k_{ba}) = (k_{ba}/RT)\mathcal{L}^{-1}\{N(t)\} \qquad (13)$$

To find the distribution as a function of the activation energy E_{ba}, A_{ba} must be known. A_{ba} is determined by measuring $N(t)$ at a number of temperatures, as will be shown below.

The inversion eq 13 can be performed analytically if the observed data can be fitted by a function $N(t)$ that can be Laplace inverted. In general, the determination of $g(k)$ or $g(E)$ must be done by computer. An approximate form for $g(k)$ is found by noting that $N_0^I(t)$ in eq 1 represents the observed curves reasonably well over a fair range in time. Inserting $N_0^I(t)$, eq 1, into eq 13 yields

$$g(k_{ba}) = \frac{(t_0 k_{ba})^n e^{-t_0 k_{ba}}}{RT\Gamma(n)} \qquad (14)$$

where $\Gamma(n)$ is the gamma function. The peak of this distribution, given by $dg/dk_{ba} = 0$, occurs at

$$k_{ba}^{peak} = n/t_0 \qquad (15)$$

By eq 2, the peak energy is related to $k_{ba}^{peak} = n/t_0$ by

$$RT \ln (n/t_0) = RT \ln A_{ba} - E_{ba}^{peak} \qquad (16)$$

The parameters n and t_0 are determined at each temperature by fitting eq 1 to the measured curves in Figures 2 and 4. A plot of $RT \ln (n/t_0)$ vs. T is shown in Figure 12 for Mb in a glycerol-water solvent. The slope of the straight line determines A_{ba}, the intercept E_{ba}^{peak}. From Figure 12, and from analogous data for MbCO in PVA, the following values are obtained:

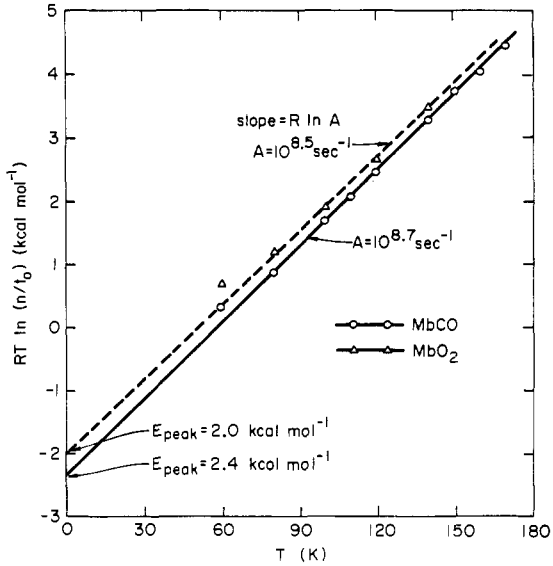

FIGURE 12: Plot of $RT \ln (n/t_0)$ vs. T determines A_{ba} and E_{peak}. MbCO and MbO_2 in glycerol-water (3:1, v/v).

$$\text{MbCO(glyc) } E_{ba}^{peak} = 2.4 \text{ kcal/mol}, \quad A_{ba} = 10^{8.7} \text{ sec}^{-1}$$
$$\text{MbO}_2\text{(glyc) } E_{ba}^{peak} = 2.0 \text{ kcal/mol}, \quad A_{ba} = 10^{8.5} \text{ sec}^{-1}$$
$$\text{MbCO(PVA) } E_{ba}^{peak} = 1.4 \text{ kcal/mol}, \quad A_{ba} = 10^{7.7} \text{ sec}^{-1} \qquad (17)$$

The statistical errors in these numbers are small; variations from sample to sample lead to an error of about ±0.2 kcal/mol in E_{ba}^{peak} and ±0.5 in log A_{ba}. With A_{ba} known, k_{ba} in eq 14 can be expressed in terms of E_{ba} and the desired $g(E_{ba})$ thus is found. This procedure can be performed at all temperatures where t_0 and n have been determined. If eq 1 were a very good approximation at all temperatures, all of these $g(E_{ba})$ should be identical. Figure 2a shows, however, that the fit is not equally good at all temperatures. We therefore use the following approach to find the "best" $g(E_{ba})$. We first determine by visual inspection the temperature at which eq 1 fits the data points best, and then compute $g(E_{ba})$ from eq 14 at this fitting temperature T_f. For all further computer calculations, we use this $g(E_{ba})$. The fitting temperature is 120 K for MbCO in glycerol-water, and 300 K for MbCO in PVA and MbO_2 in glycerol-water.

Figure 2 shows that the energy spectra thus determined must still have a shortcoming: eq 1, on which the spectra are based, fits the experimental data only to about $N(t) = 0.05$; for smaller values of $N(t)$, the experimental points fall off more rapidly than eq 1. In fact, below $N \approx 0.05$, $N(t)$ is closer to an exponential than to a power law. An exponential corresponds to one single activation energy and can be approached if the spectral function $g(E_{ba})$ cuts off at a maximum energy E_{ba}^{max}.[8] The cut-off is introduced by setting the upper limit of the integral in eq 10 equal to E_{ba}^{max}. E_{ba}^{max} is then varied till best agreement is obtained with the experimental data at all temperatures. For MbCO in glycerol-water, the cut-off energy becomes $E_{ba}^{max} = 5.4 \pm 0.2$ kcal/mol. Three energy spectra are shown in Figure 13. With these spectra and eq 10 and 17, $N(t)$ can be computed numerically at any desired temperature. As an example,

[7] Instead of eq 10, it is also possible to write $N(t) = \int_0^{\infty} dk_{ba} f(k_{ba}) e^{-k_{ba}t}$; $g(E)_{ba}$ is related to $f(k_{ba})$ by $g(E_{ba}) = -f(k_{ba})dk_{ba}/dE_{ba} = k_{ba}f(k_{ba})/RT$. At *each* temperature, $f(k_{ba})$ can be found as the Laplace inverse of $N(t)$, $f(k_{ba}) = \mathcal{L}^{-1}\{N(t)\}$. Such an inversion makes no assumption about the nature of the phenomenon giving rise to the nonexponential rebinding curves; it simply replaces one function, $N(t)$, by another one, $f(k)$. Our approach is more stringent. We must fit all data over a wide temperature range (in PVA from 40 to 350 K) with one temperature-independent energy spectrum.

[8] Of course, an abrupt cut-off as shown in Figure 13 is unnatural; a real cut-off will be smoother. However, the essential features are reproduced by the approach given here.

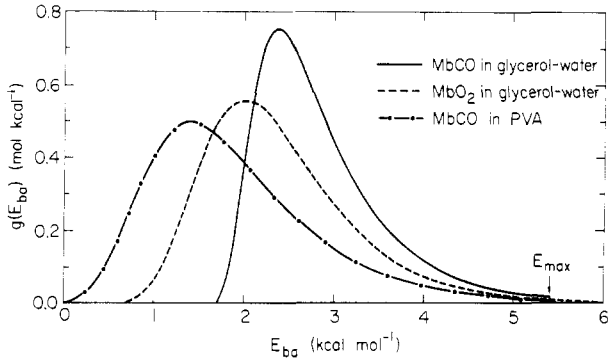

FIGURE 13: Activation energy spectra for MbCO and MbO_2.

$N(t)$ curves for MbCO in glycerol–water are shown in Figure 14. Theoretical curves and experimental points agree very well in the entire temperature range where process I can be observed, from 40 to 160 K. MbCO in aqueous solution yields an energy spectrum that is close to MbCO in glycerol–water. The energy spectrum for MbO_2 in glycerol–water displays the same general shape. The rebinding curve $N(t)$ for MbCO in PVA in Figure 4a is generally similar to that of MbCO in glycerol–water, but breaks away earlier from the horizontal and curves downward later. A good fit is obtained with the spectrum shown in Figure 14; it has a lower peak energy and higher fitting temperature than MbCO in glycerol–water.

Figure 14 demonstrates that a temperature-independent energy spectrum can explain the nonexponential rebinding curves in the temperature range from 40 to 160 K. The temperature independence of $g(E_{ba})$ can be partially checked in a different way. The rebinding at times $t \gg t_0$ is characterized by rates $k_{ba} \ll 1/t_0$ and the corresponding distribution function $g(k_{ba})$, eq 14, can be approximated by

$$g(k_{ba}) = (t_0 k_{ba})^n / RT\Gamma(n) \tag{18}$$

The spectral function $g(E_{ba})$ that governs rebinding for times $t \gg t_0$ thus becomes

$$g(E_{ba}) = \frac{(A_{ba} t_0)^n}{RT\Gamma(n)} e^{-nE_{ba}/RT}, \quad E_{ba} < E_{ba}^{max}$$
$$g(E_{ba}) = 0, \qquad E_{ba} \geq E_{ba}^{max} \tag{19}$$

If the energy spectrum is temperature independent, the approximation eq 19 should be temperature independent also and assume, for $E_{ba} < E_{ba}^{max}$, the form

$$g(E_{ba}) = \beta e^{-\alpha E_{ba}} \tag{20}$$

Here α and β are two constants defined through eq 20. Comparison of eq 19 and 20 shows that $g(E_{ba})$ can be temperature independent only if n satisfies the relation

$$n = \alpha RT \tag{21}$$

In Figure 15, n is plotted vs. T. Within errors, n is proportional to T and eq 21 is satisfied. The values of α are:

$$\begin{aligned} &\text{MbCO in: glycerol–water } \alpha = 1.4 \text{ mol/kcal} \\ &\text{water } \alpha = 1.4 \text{ mol/kcal} \\ &\text{PVA } \alpha = 1.1 \text{ mol/kcal} \\ &MbO_2 \text{ in glycerol–water } \alpha = 1.4 \text{ mol/kcal} \end{aligned} \tag{22}$$

The temperature independence of the activation energy spectrum speaks against a frequency-factor spectrum. In such an explanation, E_{ba} would have a unique value, A_{ba} would be described by a spectrum, and eq 10 would be replaced by $N(t) = \int dA_{ba} g(A_{ba}) \exp(-k_{ba} t)$. In order to fit the observed curves, A_{ba} would have to span a range from about 10^5 to 10^{20} sec^{-1} and $g(A_{ba})$ would change with temperature. Consequently we prefer a temperature-independent energy spectrum and keep A_{ba} sharp.[9]

What causes the energy spectrum? Two possibilities come to mind. (a) Each biomolecule possesses a number of sites for L in well B and the rebinding rate depends on the site occupied after the flash-off. (b) Myoglobin does not exist only in one conformation; a given primary sequence gives rise to different conformational states, with different activation energies (Klotz, 1966; Weber, 1972). To decide between these possibilities, we have performed multiple-flash experiments where successive flashes are triggered before all CO molecules have rebound. In case (a), where all Mb molecules are assumed to be identical, each successive flash would pump more ligand molecules into states with long return times, fewer ligand molecules would return fast to the binding site, and the signal would become progressively smaller. In case (b), where each Mb molecule is assumed to have one rate k_{ba}, the molecules with small k_{ba} would be removed from the game by the first flash and only the ones with large k_{ba} and hence short return times would continue to flash off and rebind. The result of a multiple-flash experiment is shown in Figure 3. During the first four flashes, the flash-off increases, indicating that the light intensity is not large enough to remove all CO at once. After the fourth flash, the behavior is repetitive and indicates that no pumping into long-lived states occurs. We consequently favor explanation (b) and assume that we deal with an assembly of Mb conformers, each with a well-defined activation energy.[10] The data do not delineate how many different states exist but the smoothness of the curves in Figures 2 and 4 indicates that there must be more than, say, ten; we assume for simplicity that the number is so large that $g(E_{ba})$ can be treated as continuous.

We finally return to the temperature dependence of the energy spectrum. Figure 14 shows that a temperature-independent $g(E_{ba})$ fits the experimental data very well. An equivalent fit is obtained by assuming the shape of $g(E_{ba})$ to be temperature independent, but that the spectrum shifts with temperature so that $E_{ba}(T) = E_{ba}(0) - S_0 T$ (A. P. Minton, private communication). We consider this possibility unlikely for the following reason. We will show in sections 7 and 8 that transitions from one conformational state to another occur with a rate given by eq 52. Below 160 K, this rate is smaller than 10^{-10} sec^{-1} so that each Mb molecule remains frozen in a given conformational state for a time long compared to our experiments and no shift of the energy spectrum occurs. The distribution of Mb molecules over all possible conformational states is *not* an equilibrium distribution but depends on the thermal history of the sample. We will return to this point in subsection 10.6.

[9] We cannot rule out the possibility that both E_{ba} and A_{ba} are continuous. The theory can be extended to this case (Primak, 1955), but we will not use this more general approach, since we can explain all data with our expressions.

[10] Actually, the result of the multiple-flash experiment is more general than stated in the text. It indicates that the activation energy spectrum is caused by a heterogeneity in the ensemble of Mb molecules. This heterogeneity can be due to conformational states, but other explanations are not excluded.

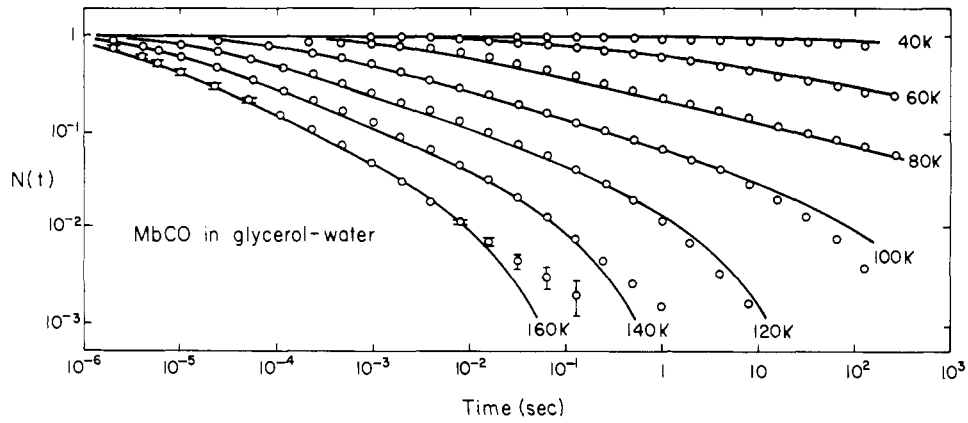

FIGURE 14: Comparison of experimental points and theoretical curves for MbCO in glycerol-water. The experimental points are the same as in Figure 2a. The solid lines are calculated from eq 10 assuming the energy spectrum given in Figure 13. Note the fundamental difference between the solid lines in Figures 2a and 14. In Figure 2a, they represent separate fits at each temperature; in Figure 14, two parameters ($g(E_{ba})$ and A_{ba}) determine all curves at all temperatures.

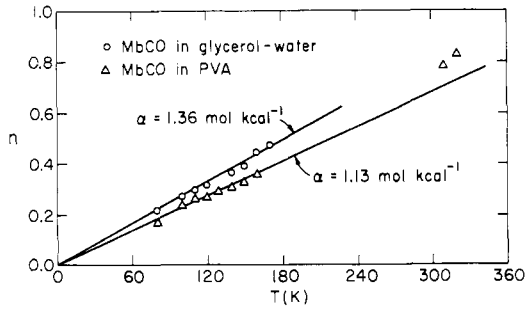

FIGURE 15: Plot of the exponent n as a function of temperature for MbCO in PVA and in glycerol-water. The fact that n follows eq 21 up to at least 200 K implies that the activation energy spectrum is unchanged to at least this temperature.

6. Binding without Diffusion and Relaxation

Between 40 and 180 K, only process I is present and the innermost barrier can thus be studied in detail and without interference from other processes. Investigation of the other barriers is complicated by two facts. All four processes may be present simultaneously, and transitions among the conformational states of Mb may affect the shape of $N(t)$. To unravel the phenomena above 180 K, we first discuss the experiments shown in Figure 4 in which MbCO is embedded in a solid matrix, PVA. Ligand diffusion into the solvent (process IV) and transitions among conformational states (relaxation) are absent. Below 180 K, the properties of barrier I can be found. Above 180 K, processes I–III are present. Since the crucial features of barrier I, $g(E_{ba})$ and A_{ba}, are known, the rates over the barriers II and III can be extracted numerically at each temperature, and the corresponding activation energies and frequency factors can be found. We describe the procedure in subsection 6.1. At temperatures above about 300 K, calculations become simpler and we treat this high-temperature limit in subsection 6.2. In subsection 6.3, we give the main conclusions.

(*6.1*) *Activation Energies and Frequency Factors.* Between about 180 and 220 K, it seems as if process I had become approximately independent of temperature, as can be seen in Figure 4. What happens is the subtle emergence of process II. The quantitative evaluation below indicates that process I continues to become faster as the temperature increases, but process II appears and simulates a slowing down of $N(t)$. At about 230 K, process III appears and by 280 K, dominates. The concentration-dependent process IV is absent in the solid matrix so that $k_{de} = 0$. We are thus left with a three-barrier problem, with the innermost barrier characterized by the activation energy spectrum $g(E_{ba})$ and the frequency factor A_{ba}.

The extraction of the rates k_{bc}, k_{cb}, k_{cd}, and k_{dc} at a given temperature from the rebinding curve $N(t)$ is performed by computer. In matrix form and with $k_{ab} = 0$, eq 5 for three barriers ($k_{de} = 0$) is

$$\mathrm{d}\mathbf{N}/\mathrm{d}t = M\mathbf{N} \tag{23}$$

where

$$\mathbf{N} = \begin{pmatrix} N_a \\ N_b \\ N_c \\ N_d \end{pmatrix}$$

$$\mathbf{M} = \begin{pmatrix} 0 & k_{ba} & 0 & 0 \\ 0 & -k_{ba} - k_{bc} & k_{cb} & 0 \\ 0 & k_{bc} & -k_{cb} - k_{cd} & k_{dc} \\ 0 & 0 & k_{cd} & -k_{dc} \end{pmatrix} \tag{24}$$

The general solution of eq 23 is found by determining the eigenvalues λ_i and eigenvectors $\mathbf{v}_i$ of the eigenvalue equation

$$(\mathbf{M} - \lambda_i \mathbf{I})\mathbf{v}_i = 0 \tag{25}$$

and expanding

$$\mathbf{N}(t) = \sum_{i=1}^{4} c_i \mathbf{v}_i e^{\lambda_i t} \tag{26}$$

$\mathbf{I}$ in eq 25 is the unit matrix. The coefficients c_1–c_4 are determined by the initial condition eq 7. The rebinding function is obtained from $\mathbf{N}(t)$ by integrating $(1 - N_a(t))$ with the proper weight $g(E_{ba})$

$$N_{calcd}(t) = \int_0^{E_{ba}{}^{max}} \mathrm{d}E_{ba} g(E_{ba})[1 - \bar{N}_a(t)] \tag{27}$$

The bar over $N_a(t)$ implies that an average over the experimental time interval has been taken. For fixed values of the rates k_{bc}, k_{cb}, k_{cd}, and k_{dc}, eq 27 yields $N_{calcd}(t)$. To obtain the actual values of the rates, the computer is instructed to fit $N_{calcd}(t)$ to the experimental points $N(t_i)$ by minimizing

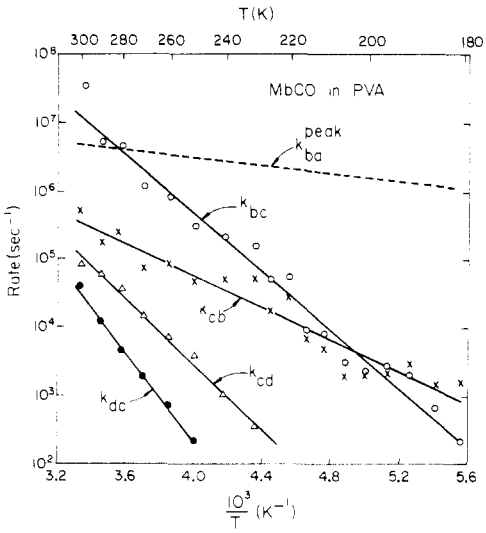

FIGURE 16: Rates for processes I–III for MbCO embedded in a solid PVA matrix. Activation energies and frequency factors deduced from these curves are given in Table II.

$$\chi^2 = \sum_{\text{all } i} \left[\frac{N(t_i) - N_{\text{calcd}}(t_i)}{\Delta N(t_i)}\right]^2 \tag{28}$$

Here $N(t_i)$ is the value of $N(t)$ measured at time t_i, with error $\Delta N(t_i)$. This procedure yields the four unknown rates at all temperatures where processes I–III are involved. The rates are plotted vs. $1/T$ in Figure 16. Slopes and intercepts give the activation energies and frequency factors for MbCO in PVA listed in Table II in section 10. With all relevant parameters of the three barriers known, the rebinding curve $N_{\text{calcd}}(t)$ at any temperature can be calculated from eq 26 and 27. A few such curves are shown in Figure 17, together with experimental points. The theoretical curves agree nearly everywhere within error with the experimental points. At a few temperatures, the experimental behavior is smoother than the theoretical one; a possible explanation will be mentioned in subsection 6.3. The curves in Figure 17 are not separate fits at each temperature; the data at *all* temperatures, from 40 to over 330 K, are faithfully reproduced with one set of activation energies and frequency factors.

(6.2) High-Temperature Limit. The numerical solution of the three-well problem provides us with rates, but not with a deeper understanding of the kinetics of the binding process and the effect of the activation energy spectrum. Fortunately, there exists a limit in which the solution of eq 5 can be found easily, namely if the outbound rates are much larger than the inbound ones:

$$k_{bc} \gg k_{ba}; \quad k_{cd} \gg k_{cb}, k_{dc} \tag{29}$$

If these conditions are satisfied, then essentially all ligand molecules placed into well B after a flash move first to well D before ultimately rebinding in well A. Figure 16 shows that eq 29 is approached above about 330 K. We call the situation where essentially all ligand molecules move to the outside before rebinding the *high-temperature limit.*

In the high-temperature limit, a quasi-equilibrium among wells B, C, and D is established rapidly after a flash, with most ligand molecules occupying well D. Rebinding to well A occurs slowly by leakage from B. The situation can be treated by the steady-state approximation where $dN_b/dt = dN_c/dt \approx 0$ and $N_a + N_d = 1$. The approximate solution to eq 5 then becomes with $k_{ab} = k_{de} = 0$

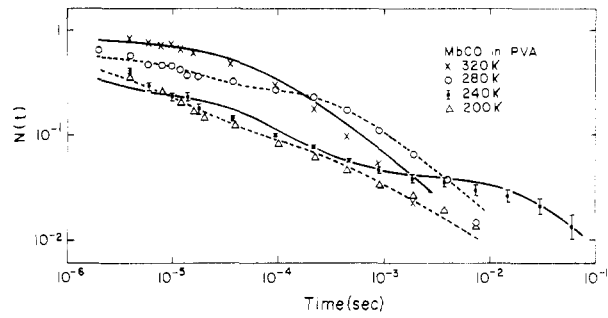

FIGURE 17: Comparison of some theoretical curves with experimental data. The experimental points are from Figure 4, the theoretical curves are computer calculations based on eq 5, the energy spectrum for PVA given in Figure 13, and the activation energies and frequency factors extracted from Figure 16. The experimental points are smoother than the theoretical curves, suggesting that also barrier II could possess an activation energy spectrum.

$$N(k_{ba},t) = 1 - N_a(t) = e^{-\lambda_{III}t} \tag{30}$$

where

$$\lambda_{III} = k_{ba}\frac{k_{cb}}{k_{bc}}\frac{k_{dc}}{k_{cd}} \tag{31}$$

For a distributed energy E_{ba}, eq 30 is generalized to

$$N^{III}(t) = \int_0^\infty dE_{ba} g(E_{ba}) e^{-\lambda_{III}t} \tag{32}$$

The factor $k_{cb}k_{dc}/k_{bc}k_{cd}$ in λ_{III} is independent of the energy E_{ba} of barrier I so that for fixed barriers II and III

$$\frac{d\lambda_{III}}{\lambda_{III}} = \frac{dk_{ba}}{k_{ba}} = -\frac{dE_{ba}}{RT} \tag{33}$$

Inserting $dE_{ba} = -RT\, d\lambda_{III}/\lambda_{III}$ into eq 32 gives as in eq 12

$$N^{III}(t) = RT\mathcal{L}\{g(\lambda_{III})/\lambda_{III}\} \tag{34}$$

In the absence of relaxation and in the high-temperature limit process III should have the same *shape* as process I. Computer calculations bear out this prediction, but it can also be verified approximately in a simpler way. The form of $g(\lambda_{III})$, without cut-off, is given by eq 14 with k_{ba} replaced by λ_{III}. The Laplace transform then gives

$$N^{III}(t) \approx (1 + t/t_0^*)^{-n} \tag{35}$$

where the parameter n is the same as for process I. A relation between n, t_0^*, and λ_{III} is obtained as in eq 15 by setting $dg/d\lambda_{III} = 0$; this condition leads to

$$\frac{n}{t_0^*} = \lambda_{III}^{\text{peak}} = \frac{k_{ba}^{\text{peak}} k_{cb} k_{dc}}{k_{bc} k_{cd}} \tag{36}$$

The parameters n and t_0^* are obtained by fitting eq 35 to the data.

(6.3) MbCO in a Solid Matrix. The results obtained with MbCO in PVA lead to the following conclusions. (i) In a solid matrix, the activation energy spectrum at the innermost barrier determines even the shape of process III, which corresponds to rebinding from the outer well D. (ii) The energy spectrum $g(E_{ba})$ is essentially unchanged up to at least 320 K. This fact can be seen from the agreement of the experimental curves with the predictions of eq 34. Moreover, the derivation leading to eq 35 implies that the exponent n should be given by eq 21 as $n(T) = \alpha RT$. Values of n for MbCO in PVA, taken from Figure 4 and

shown in Figure 15, indeed lie close to the straight line drawn through the process I data. (iii) Process III, as stated in (i), reflects the activation energy spectrum at the inner barrier. This feature supports our model in which it is assumed that the various barriers are in sequence. If process III led to rebinding by bypassing barrier I, it would be unlikely that it would display the same energy spectrum as process I. (iv) The experimental curves in Figures 4 and 17 are smooth and show little structure. The theoretical curves in Figure 17, in contrast, show small bumps that correspond to processes II and III. A smoothing of the bumps would be expected if not only barrier I, but also one or both of the other barriers were distributed in energy. It will be difficult to explore this aspect in detail. Process I occurs alone over about a factor 4 in temperature and consequently can be studied easily. Processes II and III can only be observed in a much smaller range and they never occur alone; they are also always influenced by the innermost barrier.

7. Conformational Relaxation

We have explored the properties of the barriers I–III in sections 5 and 6 and we should now turn to the outermost one. Before being able to do so, we must solve another problem. Figures 4–7 show that the rebinding of a ligand to Mb after a photoflash is exponential in a liquid sample, but close to a power law in a solid one. The difference can be understood by assuming that in solid samples each Mb molecule remains in a given conformational state whereas in a liquid one a given Mb molecule changes rapidly from one conformational state to another. We call this process conformational relaxation.

Relaxation can be characterized by a correlation time, τ_r, or rate, $k_r = 1/\tau_r$. Loosely defined, τ_r is the time required for a substantial change in the activation energy E_{ba} of a given molecule, for instance by a rearrangement in the tertiary structure. If no relaxation occurs, the rebinding process reflects the activation energy spectrum of the inner barrier and the rebinding function $N(t)$ is nonexponential. If relaxation is complete, $N(t)$ is exponential.

The influence of relaxation is easiest to discuss if process I is alone. The maximum time spent by a ligand molecule in well B before rebinding then is given by $\tau_{max} = 1/k_{ba}^{min}$, where k_{ba}^{min} is the smallest rate corresponding to the energy E_{ba}^{max} in Figure 13. In terms of rates, we have *no relaxation in process I* if

$$k_r \ll k_{ba}^{min} \tag{37}$$

In contrast, with fast relaxation, all Mb molecules undergo many conformational changes before their ligands rebind. The condition for *complete relaxation in process I* is

$$k_r \gg k_{ba}^{max} \tag{38}$$

where k_{ba}^{max} is the maximum return rate. At any time, the ensemble of Mb molecules will be in dynamic equilibrium, and the energy spectrum given by $g(E_{ba})$.[11] The number of Mb molecules with activation energies between E_{ba} and $E_{ba} + dE_{ba}$ at time t will consequently be $dN(t) = N(t)g(E_{ba})dE_{ba}$. The number of these that rebind during the time interval between t and $t + dt$ is $d(dN(t)) = -k_{ba}dN(t)dt$ or $d^2N(t) = -k_{ba}N(t)g(E_{ba})dE_{ba}dt$. Integration with the initial condition $N(0) = 1$ yields

$$N(t) = e^{-\int dE_{ba} g(E_{ba}) k_{ba} t} \equiv e^{-k_{ba}^{mean} t} \tag{39}$$

Regardless of the form of $g(E_{ba})$, rebinding in the limit $k_r \gg k_{ba}^{max}$ will be exponential. The "effective energy spectrum" thus has narrowed to a delta function and the process is similar to motional line narrowing in nuclear magnetic resonance (Bloembergen et al., 1948; Pines and Slichter, 1955). With $k_{ba}dE_{ba} = -RTdk_{ba}$, and with $g(k_{ba})$ given by eq 14, the integral can be done; the result is with eq 15 in a good approximation

$$N(t) = e^{-k_{ba}^{peak} t} \tag{40}$$

If condition (38) is satisfied, the ligand molecules will rebind exponentially with a rate corresponding to the activation energy E_{ba}^{peak}.

Another case that is easy to solve is the high-temperature limit, where again only one process dominates. As an example, we shall use the case discussed in section 6 where $k_{de} = 0$, process IV is absent, and $N(t) \simeq N^{III}(t)$. *No relaxation of process III* implies

$$k_r \ll \lambda_{III}^{min} = \frac{k_{ba}^{min} k_{cb} k_{dc}}{k_{bc} k_{cd}} \tag{41}$$

The rebinding function $N(t)$ is nonexponential and given by eq 34. *Complete relaxation in process III* implies

$$k_r \gg \lambda_{III}^{max} = \frac{k_{ba}^{max} k_{cb} k_{dc}}{k_{bc} k_{cd}} \tag{42}$$

Again, the energy spectrum of the Mb molecules will be in dynamic equilibrium and $d^2N(t) = -k_{ba}(k_{cb}k_{dc}/k_{bc}k_{cd})N(t)g(E_{ba})dE_{ba}dt$ which leads to

$$N(t) = \exp\left[-\frac{k_{cb}k_{dc}}{k_{bc}k_{cd}} \int dE_{ba} g(E_{ba}) k_{ba} t\right] \tag{43}$$

Solving the integral in eq 43 gives with eq 36

$$N(t) = e^{-\lambda_{III}^{peak} t} \tag{44}$$

and rebinding will be exponential.

Equations 40 and 44 imply that problems in which relaxation is complete are solved by the replacement

$$\int dE_{ba} g(E_{ba}) k_{ba} \rightarrow k_{ba}^{peak} \tag{45}$$

The prescription should hold even if more than one process is present.

The general solution of the intermediate case in which relaxation is present but not complete during a significant part of the rebinding process requires a theoretical model for relaxation at times near τ_r. However, for times $t \ll \tau_r$ and $t \gg \tau_r$, the solution should be model independent. We can therefore get an approximate solution for $N(t)$ and an approximate relaxation time at a given temperature by making τ_r one of the parameters in the computer fitting routine and setting up the following problem. (a) Assume no relaxation of $N(t)$ for times $t \leq \tau_r$. (b) Assume complete relaxation for times $t > \tau_r$. (c) Use the final conditions of the unrelaxed solution at $t = \tau_r$ as the initial conditions for the completely relaxed solution. This procedure will be used in section 8 for the analysis of the data in glycerol–water solvent.

8. Binding with Diffusion and Relaxation

In a liquid solvent, two phenomena can take place in ad-

[11] In contrast, if no relaxation occurs, the ensemble is not in dynamic equilibrium. At the start of the reaction, the Mb molecules that have small activation energies react first and are depleted from the ensemble represented by $g(E_{ba})$. At long times, only the high energy tail of $g(E_{ba})$ contributes to the reaction.

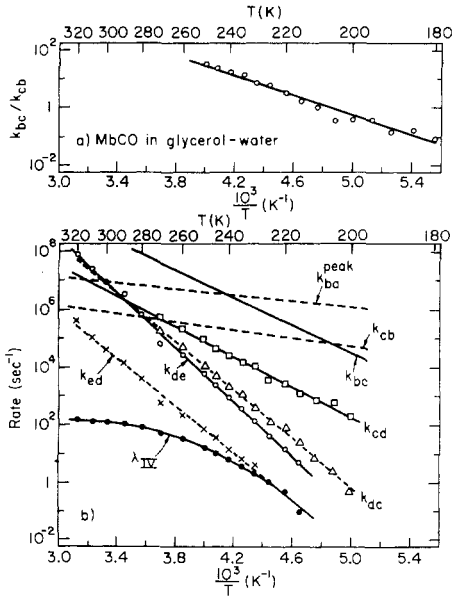

FIGURE 18: Rates for processes I–IV for MbCO in glycerol-water, 3:1, v/v. (a) Ratio of rates over barrier II, k_{bc}/k_{cb}. (b) Arrhenius plots for all rates. Note that λ_{IV}, describing the observed rate for process IV, does not describe an elementary step, as is discussed in subsection 8.1. Activation energies and frequency factors deduced from these Arrhenius plots are given in Table I. [CO] = 3×10^{-5} *M*.

dition to those discussed in section 6. (1) Some or all of the ligand molecules released by a photoflash can diffuse into the solvent. All ligand molecules in the solvent then compete for the vacant binding site. The resulting process IV thus is second order, proportional to the ligand concentration, and becomes pseudo-first-order at high ligand concentrations. (2) Conformational relaxation can set in and the rebinding curves can become exponential. The evaluation of rebinding after a photoflash must in general be performed numerically; the relevant ideas have been sketched at the beginning of section 6 and the end of section 7. Details will be given separately (Beeson, 1975). In the high-temperature limit, an explicit formula for the rebinding rate can be given. In this section, we will first treat the high-temperature limit and then present the results for MbCO and MbO_2.

(*8.1*) *The High-Temperature Limit.* We define the high-temperature limit as in eq 29 through the condition that the outbound rates are much bigger than the inbound ones:

$$k_{bc} \gg k_{ba}^{peak}; \quad k_{cd} \gg k_{cb}; \quad k_{de} \gg k_{dc}, k_{ed} \tag{46}$$

The rate λ_{IV} for process IV then follows from eq 5 as

$$\lambda_{IV} = k_{ba}^{peak} \frac{k_{cb}}{k_{bc}} \frac{k_{dc}}{k_{cd}} \frac{k_{ed}}{k_{de}} \tag{47}$$

so that

$$E_{IV} = E_{ba}^{peak} - E_{bc} + E_{cb} - E_{cd} + E_{dc} - E_{de} + E_{ed}$$

$$A_{IV} = A_{ba}A_{cb}A_{dc}A_{ed}/A_{bc}A_{cd}A_{de} \tag{48}$$

E_{IV} is the energy difference between the bottom of well E and the top of the innermost barrier, as indicated in Figure 11.

Equations 47 and 48 permit us to understand the behavior of the rate λ_{IV}. Figure 7 shows that process IV for MbCO appears at about 210 K, becomes larger as the temperature increases, and is the sole directly observable process above 270 K. In the entire temperature range IV is exponential: $N^{IV}(t) = N^{IV}(0) \exp(-\lambda_{IV}t)$. The rate λ_{IV} can be determined from Figure 7, for instance with the tool described in footnote 3, and is plotted in Figure 18b vs. $10^3/T$. The rate λ_{IV} does *not* obey an Arrhenius relation, but shows a pronounced bend centered at about 270 K. At low temperatures, the slope yields

$$E_{IV}' = 18.9 \text{ kcal/mol}, \quad A_{IV}' = 10^{18.3} \text{ sec}^{-1} \tag{49}$$

Above 300 K, the result is

$$E_{IV} = 2.9 \text{ kcal/mol}, \quad A_{IV} = 10^{4.1} \text{ sec}^{-1} \tag{50}$$

This change in apparent activation energy and frequency factor can be understood as follows. At low temperatures, around 220 K, where very few CO molecules diffuse into the solvent, their return is governed by the outermost barrier. Above 300 K, Figure 7 shows that all CO molecules leave Mb after photodissociation; the conditions for the high-temperature limit are approached or satisfied. The activation energy measured above 300 K therefore does not describe one barrier, but measures the energy difference between the bottom of well E and the top of barrier I.

(*8.2*) *MbCO in Glycerol–Water.* Rates for rebinding of CO to Mb after photodissociation, computed from the data in Figure 7, are plotted in Figure 18b vs. $10^3/T$. The elementary rates follow Arrhenius relations very well, in some cases over as many as seven decades in rate. The activation energies and frequency factors deduced from the slopes and intercepts of the various $k(T)$ are collected in Tables I and II. Conclusions will be given in section 10, but a number of remarks are in order here.

(i) In MbCO, the rates for barriers I, III, and IV can be determined unambiguously. The rates for barrier II are hard to obtain and the values for E_{bc}, E_{cb}, A_{bc}, and A_{cb} in Table I consequently have large errors. The ratio k_{bc}/k_{cb}, however, can be extracted well; it is shown in Figure 18a and yields

$$E_{bc} - E_{cb} = 7.7 \text{ kcal/mol}$$

$$A_{bc}/A_{cb} = 10^{8.2} \tag{51}$$

The difficulty of finding k_{bc} and k_{cb} separately is caused by the time limitation of our equipment and the nature of barrier II. Between 180 and 195 K, where process II can be observed well, k_{cb} is considerably larger than k_{bc} as is evident from Figure 18a. A CO molecule that jumps from well B to C returns immediately to B again. Process II therefore "hugs" process I closely and does not stand out as for instance process IV. Extension of observations to times shorter than 2 μsec would permit a much better determination of the individual rates. The inability of obtaining the separate activation energies and frequency factors for barrier II does not affect our conclusions in section 10.

(ii) Figure 7 provides evidence for conformational relaxation. Process IV is exponential at all temperatures where it can be observed well, but process II is nonexponential up to at least 230 K. The relaxation rate k_r consequently must lie between the corresponding rates. If we assume that the relaxation rate follows an Arrhenius relation, a computer fit at all temperatures is obtained by assuming

$$E_r \geq 24 \text{ kcal/mol}, \quad A_r \geq 10^{23} \text{ sec}^{-1} \tag{52}$$

(iii) The rates in Figure 18 have been obtained by assuming that conformational relaxation takes place with a single rate satisfying eq 52. All elementary rates in Figure 18 follow Arrhenius plots from 200 to 320 K. For k_{ed} and k_{de}, the

lines are straight over about seven decades. These features suggest that no major conformational change occurs in Mb in this temperature range, apart from the conformational relaxation already discussed in (ii).

(*8.3*) *MbO_2 in Glycerol–Water.* The evaluation of the O_2 data in Figures 2b and 9 proceeds as for MbCO and leads to the rates shown in Figure 19, but some special problems are involved. (i) The preparation of a ferrous MbO_2 sample is more difficult than that of MbCO and small variations from sample to sample lead to somewhat different high-temperature rebinding curves. (ii) The quantum yield for photodissociation of O_2 is substantially smaller than one and the energy of the pulsed laser is not sufficient to photodissociate all MbO_2. (iii) We have studied the optical spectrum of MbO_2 at temperatures below 10 K. The spectrum after complete photodissociation differs from that of deoxymyoglobin. The change in optical density at the monitoring wavelength, 436 nm, in going from oxymyoglobin to the photodissociated state is only 60% of the corresponding change from oxy- to deoxymyoglobin. Thus, even if all bound O_2 molecules are photodissociated, the signal observed in the photomultiplier at low temperatures is 40% smaller than at higher temperatures. We assume that the optical spectrum observed at low temperatures after flash-off is associated with well B and treat the data accordingly. (iv) Photodissociation of MbO_2 is initiated with a 590-nm (rhodamine 6G) or 540-nm (coumarin 6) dye laser. Both have disadvantages. At low temperatures, the α band in the optical spectrum of MbO_2 sharpens and the overlap with the 590-nm light decreases. The 540-nm laser gives good overlap with the β band, but the laser energy is low. Combination of the problems (ii)–(iv) results in a change in the optical density for MbO_2 that is about five times smaller than for MbCO. (v) As Figure 9 shows, process III can barely be seen. We have therefore evaluated the MbO_2 data assuming only three barriers, I, II, and IV. The identification of the barely visible process with III is based on its position in the time sequence and on the similarities of the other three with processes I, II, and IV in MbCO. Neglecting barrier III implies that the activation energy determined from the rate k_{ce} describes the transition from the bottom of well C to the top of barrier IV. (vi) As in MbCO, barrier II is not as well determined as barriers I and IV. As a result of the difficulties listed here, the barriers for MbO_2 are not as well fixed as for MbCO.

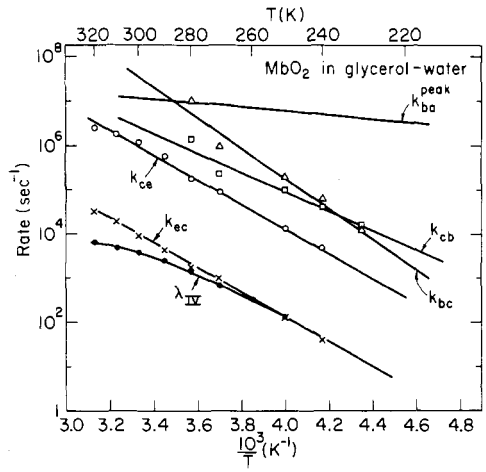

FIGURE 19: Rates for processes I, II, and IV for MbO_2 in glycerol–water, 3:1, v/v. Activation energies and frequency factors deduced from these curves are given in Table I. $[O_2] = 6 \times 10^{-5}$ *M*.

9. Activation Energies and Entropies

We present in this section the relevant equations governing rate constants and summarize activation energies and entropies of the ligand reaction with Mb. Transition-state theory (Glasstone et al., 1941) gives for the rate of a transition B → A

$$k_{ba} = \nu e^{-G_{ba}/RT} \tag{53}$$

where G_{ba} is the free-energy change between the initial state B and the transition state (intermediate state or activated complex) and ν is an approximately constant factor.[12] Expressing the free-energy change in terms of enthalpy and entropy changes, $G_{ba} = H_{ba} - TS_{ba}$, leads to

$$k_{ba} = \nu e^{S_{ba}/R} e^{-H_{ba}/RT} \tag{54}$$

We take ν, S, and H to be temperature independent and assume for a first-order transition

$$\nu = 10^{13}\ \text{sec}^{-1} \tag{55}$$

Comparison of eq 2 and 54 gives

$$H_{ba} = E_{ba}, \quad S_{ba}/R = \ln (A_{ba}/\nu) \tag{56}$$

The entropy change from B to the transition state can be obtained from the measured frequency factor by assuming $\nu = 10^{13}$ sec^{-1}. This approach is modified for process IV. The rate $k_{ed} = k_{ed}'[L]$ (eq 6) refers to a second-order reaction in a liquid (or glass). Reaction theory for this case is not well-developed (Weston and Schwarz, 1972) and the approximation we are forced to make is even cruder than eq 55. In a gas, eq 55 is replaced by

$$\nu' = 10^{14}\ \text{cm}^3/(\text{mol sec}) = 10^{11}\ (M\ \text{sec})^{-1} \tag{57}$$

where ν' refers to a second-order rate. We will use eq 57 to obtain crude values for the entropy change in the transition E → D, even though the solvent is liquid.

Activation energies, frequency factors, and entropy changes for the reaction of Mb with CO and O_2 are collected in Tables I and II. Entropy changes, obtained from eq 55–57, are listed in terms of the dimensionless quantity S/R. Most of the numbers in Tables I and II come from the experiments discussed in sections 4–8. Errors in the activation energies and frequency factors for barriers III and IV are approximately given by

$$\Delta E/E \approx \pm 0.10, \quad \Delta \log A/\log A \approx 0.10 \tag{58}$$

The corresponding relative error in (S/R) is also given by eq 58; however, the calculation of S/R rests on eq 55–57 and hence is theory dependent. Errors for barrier I are given after eq 17. Errors in the values for barrier II are considerably larger than eq 58, but the differences $E_{bc} - E_{cb}$ and $S_{bc} - S_{cb}$ have relative errors of only about 10%. Energy and entropy differences between wells B and C are thus much better known than the corresponding values for barrier II.

Data for the overall transition E → A are taken from published experiments (Keyes et al., 1971; Rudolph et al., 1972). Since these were performed in solvents different

[12] The popular relation $\nu = kT/h$, where k is Boltzmann's and h Planck's constant, predicts ν to be proportional to T. Modern treatments indicate, however, that the temperature dependence of the frequency factor is strongly model dependent (Menzinger and Wolfgang, 1969; Lin and Eyring, 1972); assuming temperature independence appears to be a good compromise.

Table I: Activation Energies (E), Frequency Factors (A), and Entropy Changes (S/R) for the Binding of CO and O_2 to Myoglobin in Glycerol–Water, 3:1, v/v.[h]

Transition[a]	Carbon Monoxide[b] E (kcal/mol)	Log A (sec^{-1})	Log A' (M sec)$^{-1}$	S/R	Dioxygen[b] E (kcal/mol)	Log A (sec^{-1})	Log A' (M sec)$^{-1}$	S/R
A → B	24[c]	16[d]		+7.1	15	13[d]		−0.3
B → A	2.4	8.7		−9.9	2.0	8.5		−10.4
B → C	11.0	16.5		+8.1	15.6	18.9		+13.6
C → B	3.3	8.3		−10.8	10.2	13.8		+1.8
C → D	12.1	15.5		+5.8				
D → C	19.3	20.9		+18.2				
D → E[f]	21.7	22.7		+22.3	12.5	15.0		+4.6
E → D[f]	18.9	18.3[e]	22.8	+27.2	12.7	13.2[e]	17.4	+14.8
E → A[g]	−21			−17	−18			−16

[a] Wells are defined in Figure 11. Unless otherwise noted, values are measured to the top of the barriers. [b] Values for CO are taken from eq 17 and Figure 18, for O_2 from eq 17 and Figure 19. [c] E_{ab} is obtained by subtraction: eq 59 with eq 48 and 50 becomes $E_{ab} = -E_{ea}{}^0 + E_{IV}$. [d] Obtained from eq 60. For O_2, $k_{ab} \approx 5k_{dis}$. [e] Pseudo-first-order rates, concentrations: [CO] = $3 \times 10^{-5} M$, [O_2] = 6×10^{-5}. [f] For O_2, values in these rows actually refer to the transitions C → E and E → C. [g] Data for the transition E → A have been taken from Keyes et al. (1971) and Rudolph et al. (1972). The values represent differences between initial and final, not transition, states. [h] Relative errors are given by eq 58 as about ±0.1 except for the transitions A → B, B → C, C → B, and E → A, where they are hard to estimate.

from ours, the values for $E_{ea}{}^0$ and $S_{ea}{}^0$ in Table I should be considered approximate. The activation energy E_{ab} is obtained by subtraction:

$$E_{ab} = -E_{ea}{}^0 + E_{ed} - E_{de} + E_{dc} - E_{cd} + E_{cb} - E_{bc} + E_{ba} \quad (59)$$

as is evident from Figure 11. Note that the energy change $E_{ea}{}^0$ and the entropy change $S_{ea}{}^0$ are *not* differences between initial and transition, but between initial and final states. The frequency factor A_{ba} is extracted from the dissociation rate. In dissociation, a ligand molecule initially in well A moves to the outside by thermally overcoming all barriers. In the high-temperature limit, a ligand that has jumped from A to B will then nearly always move to the outside; the dissociation rate k_{dis} is therefore given by the rate-limiting step A → B:

$$k_{dis} \approx k_{ab} \quad (60)$$

In general, however, k_{dis} will be smaller than k_{ab}, and k_{ab} must be found from k_{dis} and the other rates by numerically solving eq 5. Once k_{ab} is known, an approximate value for A_{ab} is determined by setting $k_{ab} = A_{ab} \exp(-E_{ab}/RT)$. The experimental values for k_{dis} at 293 K are (Antonini and Brunori, 1971) $k_{dis}(MbCO) = 0.02\ sec^{-1}$, $k_{dis}(MbO_2) = 10\ sec^{-1}$. The resulting values of A_{ab} and S_{ab}/R are given in Table I for MbCO and MbO_2 in glycerol–water. Since k_{dis} has not been measured in PVA, the corresponding values in Table II are missing.

Table II: Activation Energies (E), Frequency Factors (A), and Entropy Changes (S/R) for the Binding of Carbon Monoxide to Myoglobin Embedded in a Solid PVA Matrix.[a]

Transition	E (kcal/mol)	Log A (sec^{-1})	S/R
B → A	1.4	7.7	−12.2
B → C	9.7	14.1	+2.5
C → B	5.3	9.4	−8.3
C → D	10.9	13	0
D → C	15	15.4	+5.5

[a] Values are taken from eq 17 and Figure 16.

10. Summary and Interpretation

In the present section, we summarize and interpret the main results of our work. The section is largely self-contained, but we refer to earlier sections for amplification and proofs. In each of the eight subsections, a specific facet is described.

(10.1) Multiple Barriers. We have observed the rebinding of carbon monoxide and dioxygen to Mb after photodissociation over a wide range in temperature and time. The rebinding functions $N(t)$, displayed in Figures 4, 7, and 9, show four different processes, I–IV, characterized in section 4. With one potential barrier alone, four distinct processes cannot be explained. In section 4, we therefore have proposed a model in which four barriers are arranged in sequence, as sketched in Figure 11. In sections 5–8, we have determined all relevant barrier parameters; they are listed in Table I for MbCO and MbO_2 in glycerol–water and Table II for MbCO in a solid PVA matrix. In Figure 20a, the barriers for MbCO are drawn by giving the enthalpies H, the entropies S in units of R, and the free energies $G = H - TS$ at 310 K. The values of H, S/R, and G are only measured in the wells and at the transition states (top of the barriers); the curves are drawn to guide the eye. Figure 20b shows the corresponding wells and barriers for MbO_2.

The free energy G_{ed} and the entropy S_{ed} require one remark. The values of S_{ed}/R given in Table I are based on eq 6 and 57 and consequently imply a standard state of unit mole fraction for the ligand. G_{ed} thus also refers to the same standard state. The wells E in Figure 20 are drawn for two situations; the dashed lines refer to unit mole fraction, the solid ones to concentrations [CO] = 3×10^{-5} M and [O_2] = 6×10^{-5} M.

In Figure 21, the *free energy* for binding of CO to Mb is shown at two temperatures. At 50 K, the outer barriers dwarf the inner one; at 310 K, the inner is slightly larger than the outer ones. The change makes it clear why CO molecules in B rebind directly at low, but move preferentially to the outside at high temperatures.

In our discussions we have assumed that all four barriers are in sequence. In subsection 6.3, we have already partially justified this model by showing that the three barriers in solid PVA are likely to be in series. Figures 5 and 6 suggest that barriers III and IV are also in series: when process IV is blocked, process III is seen. Further support comes from

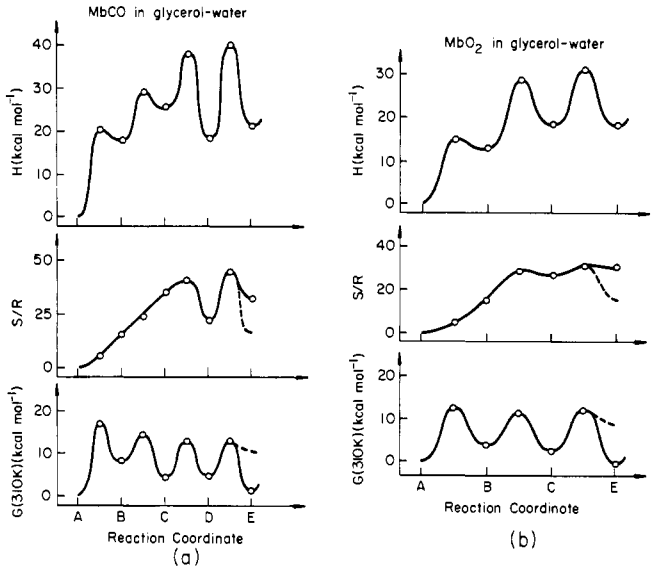

FIGURE 20: Enthalpy, entropy, and free energy (calculated at T = 310 K) as a function of reaction coordinate for (a) CO and (b) O_2 binding to Mb. The solid lines in well E for S/R and G are calculated assuming a pseudo-first-order reaction ([CO] = 3×10^{-5} M, [O_2] = 6×10^{-5} M), the dashed ones describe a second-order reaction calculated for unit mole fraction.

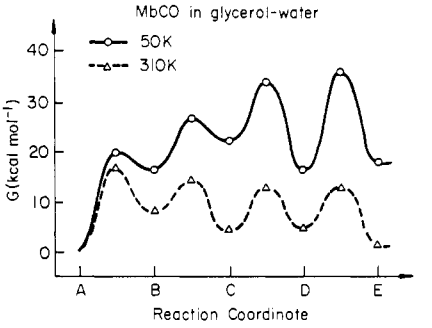

FIGURE 21: The free energy for the binding of CO to Mb as a function of reaction coordinate. At 50 K, a ligand in well B will move only to A; at 310 K, it will predominantly go to well E.

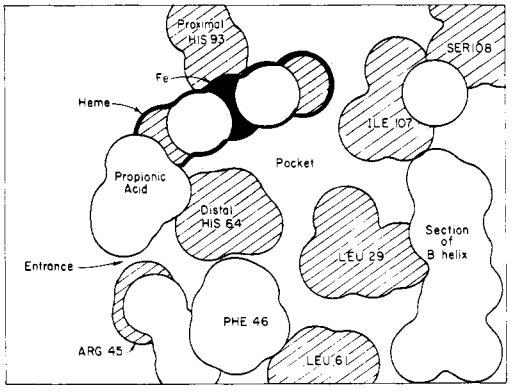

FIGURE 22: Cross section through the region near the active center of Mb. A pocket on the distal side of the heme can be entered from the outside through a narrow hole formed between His-64 and the propionic side chain. Shaded groups are in, unshaded ones above, the plane containing the iron.

consideration of all enthalpies and entropies. Equation 50 shows that the energy difference between the bottom of well E and the top of barrier I (Figure 11) can be obtained in two different ways, either from the slope of λ_{IV} in the high-temperature limit or by adding the proper energies from Table I. The first approach gives E_{IV} = 2.9 kcal/mol (eq 50), the second −0.9 kcal/mol. The two values agree within the limits of error implied by eq 58. Similarly the frequency factor $A_{IV} = 10^{4.1}$ sec^{-1} agrees well with the combination $A_{ba}A_{cb}A_{dc}A_{ed}/A_{bc}A_{cd}A_{de} = 10^{1.5}$ sec^{-1}. An additional test comes from the entropy difference between wells E and A, where the value (S/R) = −17 (Keyes et al., 1971, Rudolph et al., 1972) agrees within errors with the algebraic sum of the kinetically determined numbers from Table I, $(S/R)_{kin}$ = −18.6. Finally we note that it would be unlikely for the Arrhenius plots in Figure 18 to be straight over as many as seven orders of magnitude in rate unless the model had some validity.

Why does Mb possess multiple barriers? Efficient oxygen storage probably demands a highly ordered state. The transition from the free O_2 (or CO) in the solvent to the bound state then requires a large negative change in S. For a given k_{ba}, enthalpy changes to the transition state are connected by eq 54 as

$$\frac{H_{ba}}{RT} = \ln\left(\frac{\nu}{k_{ba}}\right) + \frac{S_{ba}}{R} \qquad (61)$$

In order to achieve a fixed reaction rate, H_{ba} must decrease with increasing order, i.e., increasing *negative* S. This consideration explains the small activation energy at the inner barrier. If no outer barriers were present, the small inner one would probably be overwhelmed by all kinds of molecules in the solvent. If this speculation is correct, then we would expect to find multiple barriers in many enzymes. Indeed, we have seen such multiple barriers in hemoglobin, the separated hemoglobin chains, carboxymethylated cytochrome *c*, and cytochrome P450 with and without camphor substrate.

(10.2) Barriers and Mb Structure. So far we have interpreted the experimental results of section 3 by postulating the existence of four barriers, but without identifying these with specific parts of Mb. X-Ray and neutron diffraction data (Kendrew et al., 1958; Watson, 1968; Schoenborn, B. P., Norwell, J., and Nunes, A. C., personal communication) provide evidence for features that could produce these wells and barriers. Figure 22 shows a cross section through part of Mb, approximately at right angles to the heme plane. The heme extends to the Mb surface, but the iron in its center is well hidden. On the distal side of the iron is a prominent pocket with linear dimensions of at least 0.5 nm lined with hydrophobic residues. The distal histidine His-64 inside the pocket is present in all mammalian Mb; its nitrogen $N_{\epsilon 2}$ is about 0.4 nm away from the heme center. The entrance to the pocket is narrow and partially blocked by the propionic side chain of the heme. The entire molecule is surrounded by a hydration shell. A plausible, but by no means unique, scenario for the binding of a ligand to Mb is as follows. Moving from the solvent (well E) toward the entrance, L first overcomes barrier IV, formed by the hydration shell. Well D thus could be between the hydration shell and the entrance to the pocket. Support for the identification of barrier IV with the hydration shell comes from experiments with heme (Alberding et al., to be published) which show two barriers, with properties similar to the Mb barriers I and IV. We therefore assign I to the heme and IV to the solvent. Barrier III could be formed by the narrow entrance to the pocket, well C by a weak bond to the surface of the cavity. Breaking this bond and thus overcoming

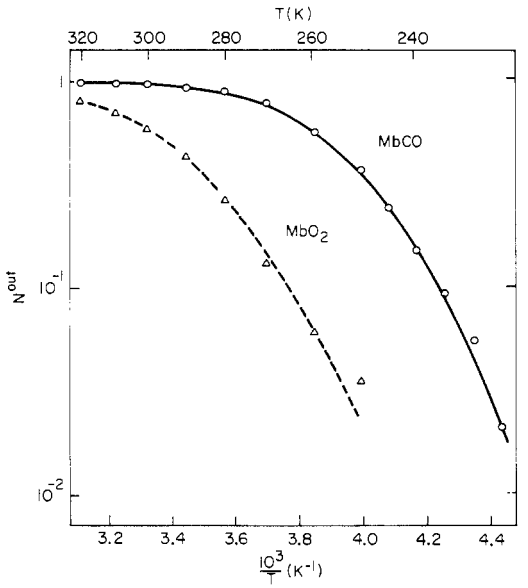

FIGURE 23: Plot of N^{out} vs. $10^3/T$. N^{out} is the total fraction of ligand molecules that do not rebind directly, but first move into the solvent.

barrier II, L moves to well B close to the heme iron and due possibly to His-64. Evidence for such an assignment comes from optical (Iizuka et al., 1974) and Mössbauer (Lang, private communication) experiments which indicate that photodissociation of CO at low temperatures does not lead to the deoxygenated form. Finally in well A, L is bound to the heme iron, and possibly also to His-64. The innermost barrier, I, could be caused by the active center since there is a connection between spin state and position of the heme iron, planarity of the heme ring, and occupation of the active site (Huber et al., 1970; Perutz, 1970). Of the six ligand positions of the iron atom, four are bound to four nitrogen atoms in the heme plane. Position 5 connects the iron to the polypeptide chain at the proximal histidine. The molecules O_2 or CO bind at position 6. X-Ray, neutron diffraction, and Mössbauer data indicate that the states of the iron and the heme depend on whether position 6 is free or occupied. The iron atom with free position 6 is displaced out of the heme plane, in a high-spin state, $S = 2$, and the heme plane is puckered. With CO or O_2 bound, the iron is more nearly in the plane, in an S=O low-spin state, and the heme plane is flat. As the ligand molecule approaches the heme center with position 6 not yet occupied, the iron must move into the plane, change spin state, and the heme must alter shape. Possibly the activation energy required for these changes accounts for the inner barrier. If so, the height of the barrier could be influenced by the protein structure via position 5 and the heme nitrogen atoms.

(*10.3*) *Specificity and Order.* Two essential attributes of enzymes are specificity and order. The native substrate is preferentially selected and guided to a state of high order. Even though Mb is not an enzyme, it illustrates how specificity and order are produced.

Specificity is studied here by comparing the binding of CO and O_2. The free-energy profiles in Figure 20 tell the following story. A CO molecule entering from the solvent encounters monotonically increasing free energy barriers. In each intermediate well the outbound rates are larger than the inbound ones: $k_{de} > k_{dc}$, $k_{cd} > k_{cb}$, and $k_{bc} > k_{ba}$. CO therefore proceeds to the binding site A by a random walk. After the first step, E → D, CO has a larger probability to return to E than to proceed to C and it takes a few tries before CO makes it to C. Once there, it is again more likely to return to D and from there to E than to continue to B. CO consequently shuttles many times among the various wells before coming to rest at the heme iron. At 310 K, the rate λ_{IV} is about 600 times smaller than k_{ed}; CO moves a few hundred times over barrier IV before binding. Binding of O_2 proceeds in a much smoother way. Barriers I and IV dominate and they have essentially equal free-energy heights, barrier II is smaller. At 310 K, λ_{IV} is only about four times smaller than k_{ed}; an O_2 molecule that moves for instance from the solvent over barrier IV has nearly equal probability of returning to the solvent or reaching the binding site A and requires only a few tries to get from E to A. Specificity in Mb thus appears to be achieved through a collaboration of active center (barrier I), globin structure (barriers II and III), and hydration shell (barrier IV). The design is optimal for rejecting the intruder CO and accepting the natural ligand O_2: CO is discriminated against at each barrier. O_2, on the other hand, moves just as easily in as out so that Mb is an efficient oxygen acceptor *and* donor. The difference between CO and O_2 can also be seen in Figure 23 which gives $N^{out}(T)$, the fraction of ligand molecules that move into the solvent after photodissociation. All CO molecules are ejected from Mb after a flash at temperatures above about 270 K. A major fraction of all O_2 molecules, however, do not leave Mb, but return directly to the binding site after each flash.

Figure 20 also shows how *order* is established. Consider a CO molecule coming from the solvent. The entropy S/R of the system Mb + CO increases over the first two barriers (IV and III) and then steadily decreases till it reaches a minimum when CO is at the binding site A. The increase in S/R at barrier IV can be due to breaking of hydrogen bonds when CO passes through the hydration shell. The increase at barrier III can be caused by breaking of bonds or displacement of residues. S/R is larger in well C than in D or E; this fact can find a natural interpretation in the size and construction of the pocket, as implied by Figure 22. The number of states, W, for the CO molecule in the pocket can be large enough so that the Boltzmann relation, $S/R = \ln W$, can explain all or part of the observed value. A contribution can also come from the interaction of the CO with the protein. A problem arises in the step B → A: it appears impossible to obtain the large entropy change, $S/R = -17$, by considering only the states of the small ligand molecule. We suggest the following explanation. In state B, the ligand molecule is bound to the partially charged nitrogen $N_{\epsilon 2}$ of the distal histidine His-64. In well A, the ligand is additionally bound to the heme iron and thus links the heme group and the distal histidine as has been suggested by Pauling (Pauling, 1964). The state B would be the precursor to the final state A; with binding enthalpy CO-$N_{\epsilon 2}$ given by $E_{bc} \simeq 11$ kcal/mol. A precursor could facilitate the final binding step, B → A, which involves a spin change of two units and thus requires presumably times of the order of nanosecond or longer. A number of observations support this model. (a) The bond Fe-CO-$N_{\epsilon 2}$ can stabilize a major part of the protein; the drop in entropy then is caused not only by restricting the states of CO but also of a number of residues, and the observed value, $S/R \approx -17$, can be explained. (b) CO fits well between the heme and His-64. Using the known positions of Fe and $N_{\epsilon 2}$ (Antonini and Brunori, 1971), a bond length of about 0.14 nm for O-$N_{\epsilon 2}$ results and this value appears reasonable. (c) It is known that CO and

O_2 stabilize heme proteins against denaturation (Cassatt and Steinhardt, 1971). A Fe-$N_{\epsilon 2}$ link could produce stabilization. (d) The stretching frequency of CO bound to Mb (1944 cm^{-1}) is considerably smaller than for CO bound to free heme (1974 cm^{-1}) or heme proteins lacking the distal histidine (1970 cm^{-1}) (Alben and Caughey, 1968; Caughey et al., 1969). Bonding with charge transfer from $N_{\epsilon 2}$ of His-64 could explain the frequency shift (Franceschetti, D. R. and Yip, K. L., to be published). (e) We have also studied low-temperature photodissociation of CO in carboxymethylated cytochrome *c* and in heme (Alberding et al., to be published). In both cases, no distal histidine is present. The frequency factor A_{ba} is of the order of 10^{12} sec^{-1}, corresponding to an entropy change $S_{ba}/R \approx 2$, considerably smaller than for Mb.

MbO_2 displays features similar to MbCO, but the entropy changes are generally smaller. Here also, the ligand O_2 could form a bridge between the heme and the distal histidine. Evidence for such a bridge has been obtained by Yonetani and coworkers in a related system, cobalt myoglobin (Yonetani et al., 1974).

(*10.4*) *Activation Energy Spectra.* At temperatures below about 180 K, only process I, the direct rebinding from B, takes place after photodissociation. Figure 21 explains that the dominance of I is due to a shrinking of the innermost and a growth of the outer free-energy barriers with decreasing temperature. Against expectation, process I is not exponential, as can be seen dramatically in Figures 2 and 4. Our explanation is to ascribe the observed time dependence $N(t)$ to the existence of an energy spectrum at the inner barrier. From $N(t)$, the spectral distribution $g(E_{ba})$ can be found and it is given for CO and O_2 in Figure 13. The result of a multiple flash experiment, Figure 3, demonstrates that the activation energy spectrum must be due to a heterogeneity in the ensemble of Mb molecules.

We have already made some comments concerning the activation energy spectrum in section 5, and add some further remarks here. (a) Nonexponential rebinding at low temperatures occurs not only in Mb, but in all heme proteins that we have studied so far (N. Alberding et al., to be published). The energy spectra depend strongly on the protein and differ, for instance, considerably for the separated α and β chains of hemoglobin. Substrate also affects the spectrum and cyt P450 with and without the camphor substrate display very different spectra. Low-temperature spectra thus may become useful for fingerprinting proteins. (b) The innermost barrier can be studied extremely well because it can be seen alone over an enormous temperature range (in Mb from 40 to 160 K) and because $N(t)$ extends at most temperatures over more than six orders of magnitude in time. The other barriers cannot be investigated in similar detail and it is not possible to assert unambiguously that they are described by only one energy. In fact, some tentative evidence in section 6 suggests that at least barrier II is also distributed. (c) The solid lines in Figure 14 are based on the energy spectrum for MbCO in glycerol-water shown in Figure 13. The curves are *not* separate fits at each temperature. One measurement of $N(t)$ at one temperature yields $g(k_{ba})$ through eq 11; a second temperature fixes A_{ba}. The energy spectrum $g(E_{ba})$ is then known and all curves at any desired temperature are unambiguously predictable. In this sense the fit in Figure 14 is given by two parameters, the shape of $g(E_{ba})$ and A_{ba}; the curves represent the experimental data extremely well over an enormous range in $N(t)$, t, and T. (d) We based the determination of $g(E_{ba})$ on eq 1. This approximation works well for Mb, but is less satisfactory for some other proteins and should not be considered a universal solution. For some proteins, it may be better to guess a $g(E)$ and then let a computer generate $N(t)$ curves through eq 10. The function $g(E_{ba})$ is then varied till a good fit is obtained at all temperatures. (e) In some proteins, return after photodissociation can be observed below 2 K. The observed $N(t)$ curves can only be explained by eq 10 down to about 20 K. At lower temperatures, marked deviations occur which we ascribe to tunneling of either CO or Fe (N. Alberding et al., to be published).

(*10.5*) *Conformational Relaxation.* An attractive explanation for the energy spectrum is the existence of many different conformational states of Mb. At low temperatures or in a solid matrix, transitions from one conformation to another are extremely slow and each Mb molecule remains in a particular state, with a corresponding value of the activation energy. At temperatures above about 230 K in glycerol-water, relaxation sets in and each molecule changes rapidly from one state to another. Absence or presence of relaxation can be determined from the shape of the function $N(t)$; complete relaxation implies exponential $N(t)$ as eq 44 proves. The relaxation rate for MbCO in glycerol-water is characterized by the values $E_r \gtrsim 24$ kcal/mol, $A_r \gtrsim 10^{23}$ sec^{-1}, as given in eq 52. The denaturation enthalpy of Mb has been determined approximately as $H_{den} = 40$ kcal/mol (Hermans and Acampora, 1967). It is therefore tempting to speculate that conformational relaxation as observed in our experiments is connected to denaturation.

One question is raised by the suggestion in subsection 10.3 that ligands stabilize the protein. If stabilization indeed occurs, it will probably also affect conformational relaxation, and the relaxation process may be different depending on whether or not a ligand is in well A. Investigations of relaxation rates with independent tools could clarify this point.

The connection between relaxation and diffusion also deserves more attention. The extremes are clear. In a solid surrounding, both diffusion and relaxation are absent, as is seen in section 6. At high temperatures and in proper liquid solvents, diffusion is present (process IV can be seen) and relaxation is rapid (all observed rebinding curves are exponentials). In liquid PVA, however, diffusion can be absent while relaxation still persists (Figure 6).

(*10.6*) *Conformational Energy.* The total free energy of an Mb molecule in a given conformational state j can be denoted by F_j. The equilibrium number of Mb molecules in state j at temperature T will be proportional to the Boltzmann factor $\exp(-F_j/RT)$. To find F_j, we assume that each conformational state j gives rise to a unique activation energy E_{ba}; we can then label the states F_j with the corresponding activation energy E_{ba} and replace F_j by $F(E_{ba})$. To get the explicit form of $F(E_{ba})$, we consider the energy spectrum for MbCO in Figure 13. According to our assumption, the spectrum represents a Boltzmann distribution in a potential well described by $F(E_{ba})$. The temperature at which the distribution is established follows from eq 52. In a typical experiment with a glycerol-water solvent, about 10^3 sec are required to cool the sample to below about 200 K. Equation 52 implies that $k_r < 10^{-3}$ sec^{-1} at about 200 K. The distribution will therefore freeze at about $T_0 =$ 200 K, and $g(E_{ba})$, normalized to $F(E_{ba}{}^{peak}) = 0$, will be given by

$$g(E_{ba},T_0) = g(E_{ba}{}^{peak}) \exp[-F(E_{ba})/RT_0] \quad (62)$$

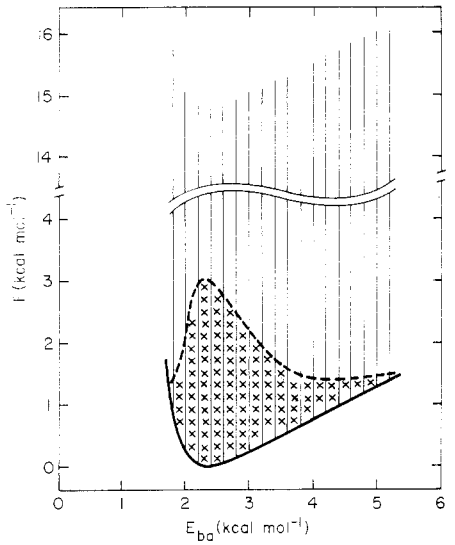

FIGURE 24: Conformational energy F_j as a function of the activation energy E_{ba}. The spikes represent the energy barriers in relaxation. The crosses correspond to a Boltzmann equilibrium distribution at 200 K.

With $g(E_{ba},T_0)$ from Figure 13, $F(E_{ba})$ can be calculated numerically; the result is displayed in Figure 24. The solid line represents $F(E_{ba})$, and the spikes are the barriers (activation energies) that have to be overcome in conformational relaxation. The crosses show a Boltzmann equilibrium distribution at 200 K. As the temperature is lowered below 200 K, the Mb molecules remain frozen in their states and this distribution remains unchanged. In contrast, as the temperature rises above 200 K relaxation sets in, Mb molecules jump over the barriers, and the distribution assumes the equilibrium shape corresponding to the ambient temperature T.

(*10.7*) *Influence of Solvent and Relaxation.* The dynamical action of Mb cannot be treated without considering the solvent an integral part of the system. The following examples bear out this assertion. (a) The outermost barrier is intimately connected to the properties of the solvent and it may, in fact, be produced by the hydration shell (subsection 10.2). Changes in the solvent thus will affect the rebinding directly. (b) The surrounding can prevent diffusion into the solvent and thus block the interchange between the interior of the biomolecule and the outside. An example is shown in Figure 6: PVA, before it hardens, permits relaxation, but process IV is absent. In solid surroundings, both relaxation and diffusion are stopped, as is shown in Figures 5 and 6. (c) Activation energies and frequency factors for the various barriers are considerably different in solid PVA and in liquid glycerol–water, as is illustrated by Figures 16 and 18. (d) The inner parts of the protein are better shielded than the outer ones. To demonstrate this trend, we give in Table III the rates at 310 K for MbCO in solid PVA and in liquid glycerol–water. The ratio of rates in the two solvents shows that the core, near the active center, is only slightly affected while the outer barriers are strongly changed. (e) As Table III shows, the rates in the liquid surrounding are larger than in the solid one; relaxation makes access to the active center easier. Nevertheless, Mb does not behave like a sieve and the path to the binding site is well controlled as is demonstrated by Figures 18 and 19.

(*10.8*) *Low-Temperature Biochemistry.* Our work implies that it is not possible to understand the dynamics of ligand binding to Mb if measurements are taken only in a narrow temperature interval, say between 278 K ($10^3/T$ = 3.6 K^{-1}) and 320 K ($10^3/T$ = 3.13 K^{-1}). Some examples will prove this assertion. (a) Between 278 and 320 K, only one process is observed after a photoflash; its rate, denoted by λ_{IV}, is shown in Figure 18 for CO and Figure 19 for O_2. If only points between 278 and 320 K are considered, the curvature in λ_{IV} is overlooked and activation energies of 3 and 6 kcal/mol are obtained for CO and O_2, respectively. They would be interpreted as barrier heights in a single-step process. Our investigation shows, however, that the binding process involves at least four barriers and that the activation energies observed at high temperatures must be broken down into individual components. In the high-temperature limit, defined by eq 46, the observed activation energies and frequency factors are given by eq 48. (b) Figure 18 shows that nearly all rates are approximately equal near physiological temperatures (compensation effect). The one rate that is much smaller, k_{ed}, is a second-order rate and depends on the ligand concentration. It can therefore also be shifted toward $k \approx 10^7$ sec^{-1} if desired. The fact that all relevant rates are approximately equal implies that there is not one rate-limiting step, but that all barriers must be taken into account in any discussion of CO binding. The rebinding curves in Figure 7 show only one process near 310 K; the complex interplay among barriers is hidden. Only if a wide temperature range is studied can the various processes be separated. (c) Figure 23 displays the fraction of ligand molecules that do not rebind directly after a flash, but move outside Mb. For CO, this fraction is very close to 1 above 278 K and the existence of the fast process I would be difficult to detect. For O_2 process I still contributes a considerable fraction at high temperatures and probably has been seen in fast laser-flash work (Alpert et al., 1974). Without low-temperature data, however, the interpretation is difficult. These three examples suggest that the investigation of biochemical reactions in many systems will require experiments extending over a wide range in temperature even though the actual physiological range is small.

Table III: Comparison of the Rates for Binding of CO to Mb in PVA (Solid) and Glycerol–Water (3:1, v/v) at 310 K.

Transition Barrier	Rate	Log Rate (sec^{-1}) PVA	Log Rate (sec^{-1}) Glycerol–Water	Ratio of Rates in Glycerol–Water to PVA
I	k_{ba}^{peak}	6.7	7.0	2
II	k_{bc}	7.3	(8.8)	(30)[a]
	k_{cb}	5.6	(6.0)	(2.5)[a]
	k_{bc}/k_{cb}	1.7	2.7	10
III	k_{cd}	5.3	6.9	40
	k_{dc}	4.8	7.3	320
IV	k_{de}	0	7.4	∞

[a] Rates in parentheses have larger errors than the other ones.

Acknowledgments

Many of our friends have helped us during the course of this work by guiding us through unfamiliar terrain, scrutinizing our ideas, pointing out related research, or generously loaning us equipment. We should like to thank all of them very much, in particular we express our appreciation to J. O. Alben, N. Alberding, S. S. Chan, P. G. Debrunner, G. DePasquali, I. Dezsi, P. Douzou, H. G. Drickamer, M. Eigen, C. P. Flynn, D. R. Franceschetti, V. I. Goldanskii, M. Gouterman, J. S. Koehler, D. Lazarus, V. P. Marshall,

R. A. Marcus, A. P. Minton, T. M. Nordlund, J. Norvell, T. Pederson, D. G. Ravenhall, J. R. Schrieffer, C. P. Slichter, and L. Sorensen.

References

Alben, J. O., and Caughey, W. S. (1968), *Biochemistry 7,* 175.

Alpert, B., Banerjee, R., and Lindqvist, L. (1974), *Proc. Natl. Acad. Sci. U.S.A. 71,* 558.

Antonini, E., and Brunori, M. (1971), Hemoglobin and Myoglobin in Their Reactions with Ligands, Amsterdam, North-Holland Publishing Co.

Austin, R. H., Beeson, K., Eisenstein, L., Frauenfelder, H., Gunsalus, I. C., and Marshall, V. P. (1973), *Science 181,* 541.

Austin, R. H., Beeson, K., Eisenstein, L., Frauenfelder, H., Gunsalus, I. C., and Marshall, V. P. (1974), *Phys. Rev. Lett. 32,* 403.

Beeson, K. W. (1975), Unpublished Thesis; available as Technical Report from the Department of Physics, University of Illinois at Urbana—Champaign, Urbana, Ill.

Bloembergen, N., Purcell, E. M., and Pound, R. V. (1948), *Phys. Rev. 73,* 679.

Bohon, R. L., and Conway, W. T. (1972), *Thermochim. Acta 4,* 321.

Cassatt, J. C., and Steinhardt, J. (1971), *Biochemistry 10,* 264.

Caughey, W. S., Alben, J. O., McCoy, S., Boyer, S. H., Charache, S., and Hathaway, P. (1969), *Biochemistry 8,* 59.

Chance, B., Schoener, B., and Yonetani, T. (1965), in Oxidase and Related Redox Systems, King, T. E. Mason, H. S., and Morrison, M., Ed., New York, N.Y., Wiley, p 609.

Cooke, R., and Kuntz, I. D. (1974), *Annu. Rev. Biophys. Bioeng. 3,* 95.

Frauenfelder, H. (1973), *Moessbauer Eff. Proc. Int. Conf. 5th,* 401.

Gibson, Q. H. (1956), *J. Physiol. 134,* 112.

Glasstone, S., Laidler, K. J., and Eyring, H. (1941), The Theory of Rate Processes, New York, N.Y., McGraw-Hill.

Hermans, J., and Acampora, G. (1967), *J. Am. Chem. Soc 89,* 1547.

Hills, B. A. (1973), *Science 182,* 823.

Huber, R., Epp, O., and Formanek, H. (1970), *J. Mol. Biol. 52,* 349.

Iizuka, T., Yamamoto, H., Kotani, M., and Yonetani, T. (1974), *Biochim. Biophys. Acta 371,* 126.

Kendrew, J. C., Bodo, G., Dintzis, H. M., Parrish, R. G., and Wyckoff, H. (1958), *Nature (London) 181,* 662.

Keyes, M. H., Falley, M., and Lumry, R. (1971), *J. Am. Chem. Soc. 93,* 2035.

Klotz, I. M. (1966), *Arch. Biochem. Biophys. 116,* 92.

Kuntz, I. D., and Kauzmann, W. (1974), *Adv. Protein Chem. 28,* 239.

Lin, S. H., and Eyring, H. (1972), *Proc. Natl. Acad. Sci. U.S.A. 69,* 3192.

Macdonald, J. R. (1962), *J. Chem. Phys. 36,* 345.

Macdonald, J. R. (1963), *J. Appl. Phys. 34,* 538.

Macdonald, J. R. (1964), *J. Chem. Phys. 40,* 1792.

Menzinger, M., and Wolfgang, R. (1969), *Angew. Chem., Int. Ed. Engl. 8,* 438.

Pauling, L. (1964), *Nature (London) 203,* 182.

Perutz, M. F. (1970), *Nature (London) 228,* 726.

Pines, D., and Slichter, C. P. (1955), *Phys. Rev. 100,* 1014.

Primak, W. (1955), *Phys. Rev. 100,* 1677.

Rudolph, S. A., Boyle, S. O., Dresden, C. F., and Gill, S. J. (1972), *Biochemistry 11,* 1098.

Theorell, H. (1934), *Biochem. Z. 268,* 73.

Wagner, K. W. (1913), *Ann. Physik. 40,* 817.

Watson, H. C. (1968), *Prog. Stereochem. 4,* 299.

Weber, G. (1972), *Biochemistry 11,* 864.

Weissbluth, M. (1974), Hemoglobin, New York, N.Y., Springer-Verlag.

Weston, R. E., and Schwarz, H. A. (1972), Chemical Kinetics, Englewood Cliffs, N.J., Prentice-Hall.

Wittenberg, J. B. (1970), *Physiol. Rev. 50,* 559.

Yonetani, T., Yamamoto, H., and Iizuka, T. (1974), *J. Biol. Chem. 249,* 2168.

Zerner, M., Gouterman, M., and Kobayashi, H. (1966), *Theor. Chim. Acta 6,* 363.